JGR Earth Surface

RESEARCH ARTICLE
10.1029/2023JF007101

Scale-Dependent Influence of Permafrost on Riverbank Erosion Rates

Joel C. Rowland[1], Jonathan P. Schwenk[1], Eitan Shelef[2], Jordan Muss[3], Daniel Ahrens[4], Sophie Stauffer[1], Anastasia Pilliouras[5], Benjamin Crosby[6], Austin Chadwick[7], Madison M. Douglas[7], Preston C. Kemeny[7], Michael P. Lamb[7], Gen K. Li[8], and Lawrence Vulis[9]

[1]Earth and Environmental Sciences Division, Los Alamos National Laboratory, Los Alamos, NM, USA, [2]Department of Geology and Environmental Science, University of Pittsburgh, Pittsburgh, PA, USA, [3]General Atomics Commonwealth Computer Research, Inc., Charlottesville, VA, USA, [4]Stanford Law School, Stanford, CA, USA, [5]Department of Geosciences, Pennsylvania State University, University Park, PA, USA, [6]Department of Geosciences, Idaho State University, Pocatello, ID, USA, [7]Division of Geological and Planetary Sciences, California Institute of Technology, Pasadena, CA, USA, [8]Department of Earth Science, University of California Santa Barbara, Santa Barbara, CA, USA, [9]Department of Civil and Environmental Engineering, University of California Irvine, Irvine, CA, USA

Key Points:

- Permafrost systematically reduces riverbank erosion rates by up to nine times compared to rivers not in permafrost regions
- The influence of permafrost on small rivers is limited and increases with river size
- Permafrost thaw due to climate change will likely increase erosion rates on large rivers and have a limited impact on smaller rivers

Supporting Information:

Supporting Information may be found in the online version of this article.

Correspondence to:

J. C. Rowland,
jrowland@lanl.gov

Citation:

Rowland, J. C., Schwenk, J. P., Shelef, E., Muss, J., Ahrens, D., Stauffer, S., et al. (2023). Scale-dependent influence of permafrost on riverbank erosion rates. *Journal of Geophysical Research: Earth Surface*, *128*, e2023JF007101. https://doi.org/10.1029/2023JF007101

Received 3 FEB 2023
Accepted 27 JUN 2023

Author Contributions:

Conceptualization: Joel C. Rowland, Jonathan P. Schwenk, Anastasia Pilliouras
Data curation: Joel C. Rowland, Jonathan P. Schwenk, Daniel Ahrens, Sophie Stauffer, Anastasia Pilliouras
Formal analysis: Joel C. Rowland, Jonathan P. Schwenk, Eitan Shelef, Daniel Ahrens, Sophie Stauffer, Anastasia Pilliouras, Madison M. Douglas, Lawrence Vulis
Funding acquisition: Joel C. Rowland, Benjamin Crosby, Michael P. Lamb

Abstract

Whether permafrost systematically alters the rate of riverbank erosion is a fundamental geomorphic question with significant importance to infrastructure, water quality, and biogeochemistry of high-latitude watersheds. For over four decades, this question has remained unanswered due to a lack of data. Using remotely sensed imagery, we addressed this knowledge gap by quantifying riverbank erosion rates across the Arctic and subarctic. To compare these rates to non-permafrost rivers, we assembled a global data set of published riverbank erosion rates. We found that erosion rates in rivers influenced by permafrost are on average nine times lower than non-permafrost systems; erosion rate differences increase up to 40 times for the largest rivers. To test alternative hypotheses for the observed erosion rate difference, we examined differences in total water yield and erosional efficiency between these rivers and non-permafrost rivers. Neither of these factors nor differences in river sediment loads provided compelling alternative explanations, leading us to conclude that permafrost limits riverbank erosion rates. This conclusion was supported by field investigations of rates and patterns of erosion along three rivers flowing through discontinuous permafrost in Alaska. Our results show that permafrost limits maximum bank erosion rates on rivers with stream powers greater than 900 Wm^{-1}. On smaller rivers, however, hydrology rather than thaw rate may be the dominant control on bank erosion. Our findings suggest that Arctic warming and hydrological changes should increase bank erosion rates on large rivers but may reduce rates on rivers with drainage areas less than a few thousand km^2.

Plain Language Summary

The rate rivers erode their banks controls the pace of migration and the impacts on neighboring communities and ecosystems. Erosion of floodplains releases sediment, carbon, and other constituents into rivers affecting the biogeochemistry of rivers and ultimately the coastal oceans into which rivers flow. Across the Arctic, rivers erode through floodplains frozen continuously for more than 2 years (permafrost). Before ice-bounded sediments can be eroded by flowing water, they must be thawed. Using aerial photographs, satellite imagery, and direct field observations, we found that permafrost slows the rate rivers erode their banks relative to rivers without permafrost. The effect of permafrost, however, varies with the size of the river and the erosion rates of large rivers are disproportionately slowed by permafrost. As a result, permafrost thaw due to climate change will likely increase erosion rates on large rivers and have limited impact on small rivers, but very little data are available for small rivers in the Arctic, highlighting key data need.

1. Introduction

At water level, the erosion of frozen bank materials by rivers leaves distinctive geomorphic features indicative of the presence of permafrost (ground that remains below 0°C for two or more consecutive years). These features include thermal-erosion niching (bank undercutting), massive cantilever failures in non-cohesive sediments, and exposed ground ice (Figure 1). From above and at larger spatial scales, however, no clear geomorphic signature of permafrost has been documented in river planform (McNamara & Kane, 2009). Due to this lack of a planform signature of permafrost on rivers, an examination of riverbank erosion rates is required to answer the fundamental

Investigation: Joel C. Rowland, Jonathan P. Schwenk, Eitan Shelef, Daniel Ahrens, Sophie Stauffer, Anastasia Pilliouras, Benjamin Crosby, Austin Chadwick, Madison M. Douglas, Gen K. Li
Methodology: Joel C. Rowland, Eitan Shelef, Jordan Muss, Daniel Ahrens, Anastasia Pilliouras, Lawrence Vulis
Project Administration: Joel C. Rowland
Resources: Joel C. Rowland, Anastasia Pilliouras, Benjamin Crosby
Software: Joel C. Rowland, Jonathan P. Schwenk, Jordan Muss
Supervision: Joel C. Rowland
Validation: Joel C. Rowland, Jonathan P. Schwenk
Visualization: Joel C. Rowland
Writing – original draft: Joel C. Rowland, Jonathan P. Schwenk, Eitan Shelef, Jordan Muss, Anastasia Pilliouras
Writing – review & editing: Joel C. Rowland, Jonathan P. Schwenk, Eitan Shelef, Jordan Muss, Daniel Ahrens, Sophie Stauffer, Anastasia Pilliouras, Benjamin Crosby, Austin Chadwick, Madison M. Douglas, Preston C. Kemeny, Michael P. Lamb, Gen K. Li, Lawrence Vulis

question: Does the presence of permafrost have an observable effect on river dynamics? For over 40 years studies of individual rivers that flow through floodplains with permafrost have observed possible, though often contradictory, influences of frozen sediment and ice on the rates of riverbank erosion (Chassiot et al., 2020; Debol'skaya & Ivanov, 2020; Gatto, 1984; Gautier et al., 2021; Lawson, 1983; McNamara & Kane, 2009; Scott, 1978; Tananaev, 2016). The lack of long-term and large-scale observations continues to hinder the assessment of the role of permafrost in riverbank erosion (Chassiot et al., 2020; Debol'skaya & Ivanov, 2020; Gautier et al., 2021; Tananaev, 2016).

The potential influence of permafrost on the rates of riverbank erosion has great relevance to communities in the Arctic. Locally, Arctic rivers are major transportation arteries and provide significant food resources to local populations (Brinkman et al., 2016; Cold et al., 2020; Hovelsrud et al., 2011; Instanes et al., 2016; Payne et al., 2018). Bank erosion in these systems threatens to undermine infrastructure (University of Alaska Fairbanks Institute of Northern Engineering et al., 2019) and cause village relocations, especially in Alaska (Figures S2 and S3 in Supporting Information S1), where 43% of villages are located less than 1 km from riverbanks (Text S1 and Figure S1 in Supporting Information S1).

Changes in bank erosion rates could substantially alter sediment and biogeochemical fluxes to the ocean. Presently, Arctic rivers have low sediment loads (Rachold et al., 2004), accounting for 10% of the global river discharge to oceans (Holmes, McClelland, et al., 2012) but only 1% of the global sediment flux (Gordeev, 2006). Rivers influence Arctic biogeochemical fluxes (Drake et al., 2018; Schuur et al., 2015; Tank et al., 2012) and may change in response to the warming climate (Holmes, Coe, et al., 2012) and feedback on atmospheric chemistry. Currently, Arctic rivers account for approximately 8% of the total organic carbon flux to global oceans (Rachold et al., 2004) and export 34 Tg of dissolved organic carbon (Holmes, McClelland, et al., 2012) and 5.8 Tg of particulate organic carbon (POC) (McClelland et al., 2016) each year.

Studies of Arctic river chemistry suggest that bank erosion contributes a significant fraction of riverine POC (Striegl et al., 2007) and that bank-derived carbon influences the age and composition of carbon in both rivers and the Arctic ocean basin (Gustafsson et al., 2011; Mann et al., 2015; Wild et al., 2019). Recent modeling studies suggest that riverine fluxes of carbon and nutrients play a significant role in the net primary productivity of the Arctic Ocean (Terhaar et al., 2021).

River migration and floodplain erosion strongly influence carbon cycling in watersheds (Torres et al., 2017). However, studies in Alaska conflict regarding the extent to which river migration influences floodplain carbon storage. A Yukon River study of the variability of floodplain carbon suggested that river migration was an important control on floodplain carbon storage (Lininger et al., 2018, 2019), while a study of the Koyukuk River, AK showed little difference in carbon quantity or characteristics between eroding banks and newly deposited point bars (Douglas et al., 2022).

Here, we present the results of a study aimed at addressing the long-standing uncertainty regarding the role of permafrost on the relative rates of riverbank erosion by evaluating rates and patterns of riverbank erosion across spatial scales ranging from individual bends to the entire Arctic and temporal scales of minutes to decades. At the largest spatial and temporal scales, we relied on remotely sensed erosion rates measured along thousands of kilometers of Arctic and sub-Arctic rivers over more than 40 years. We used field observations of active bank erosion, presence of permafrost, temperature, and bank sedimentology and ice content along the Koyukuk, Selawik, and Yukon Rivers in Alaska to quantify the role of permafrost in riverbank erosion at the smallest scales. While the heterogeneities controlling bank erosion prevent simple projections regarding the fate of permafrost-affected rivers under a warming climate, our results highlight important climate-influenced drivers and responses and reveal critical data gaps that will need to be addressed to improve such predictions.

2. Background and Motivating Hypotheses

Here we review why prior studies have reached contradictory conclusions regarding the influence of permafrost on the rates of riverbank erosion. Permafrost alters the hydrology, vegetation, and geomechanics of riverbanks in ways that may influence riverbank erosion. Hydrologically, permafrost limits water infiltration and liquid saturation of soils to a seasonally thawed shallow surface layer (French, 2007; Hinzman et al., 2005; Woo & Winter 1993) and prevents the periodic saturation and draining of riverbank faces that can lead to pore pressure-driven bank collapse commonly observed in seasonally unfrozen banks (Darby & Thorne, 1996; Rinaldi

Figure 1. Images of riverbanks eroding permafrost. (a) Thermal-erosion niche undercutting a bank composed of frozen sand along the Yukon River, in central AK. (b) Massive failure blocks resulting from thermal erosion undercutting of banks along the Yukon River, AK (66.33°N, 147.60°W). The top of the bank is approximately 4 m above the waterline. (c) Exposed ice wedge and associated bank erosion in the banks of the Yukon River, AK. (d) Thermal denudation and collapse of an ice-rich bank along the Koyukuk River (65.780°N, 156.437°W). Shovel handle in the center of photo for scale. (e) Sediments piled up on riverbank due to river ice erosion and sediment transport on the Yukon River, AK. (f) Riverbank along the Selawik River in July 2012 showing loose thawed gravels and tundra blocks from spring bank erosion protecting the bank face (66.48°N, 157.71°W). Location of images shown in Figure 3.

& Casagli, 1999; Tananaev & Lotsari, 2022; Zhao et al., 2022). The role of vegetation in stabilizing riverbanks (Simon & Collison, 2002) may be limited by permafrost restricting rooting depth to shallow seasonally thawed surface layers (Blume-Werry et al., 2019; Jackson et al., 1996), although mats of attached overhanging tundra may offer seasonal protection from erosion along smaller rivers (Walker et al., 1987).

Geomechanically, frozen pore waters provide additional strength to the soil matrix relative to the same material in an unfrozen state (Cooper & Hollingshead, 1973; Lawson, 1983; Shur et al., 2002; Tsytovich, 1975; Williams & Smith, 1991). This additional strength and cementation of grains by ice requires that the frozen sediments thaw before being physically eroded by water (Are, 1983; Randriamazaoro et al., 2007; Shur et al., 2002; Walker et al., 1987). Therefore, the rate of bank erosion may be set by the combined effects of thermal and physical processes. The thaw rates of frozen sediments decrease with increasing ice content (Randriamazaoro et al., 2007; Shur et al., 2002; Williams, 1952), and increase with larger grain sizes (Scott, 1978; Shur et al., 2002), river discharge, and water temperature (Shur et al., 2002), with greater sensitivity to temperature than discharge (Costard et al., 2003; Dupeyrat et al., 2011; Randriamazaoro et al., 2007). Though thaw rates may slow with increasing ice content, ice in excess of the sediment pore volume may augment net erosion rates for some deposits relative to similar unfrozen, ice-free materials (Gatto, 1984; Shur et al., 2002) due to a loss of cohesion upon thawing (Dupeyrat et al., 2011) and/or because the volume of sediment to be eroded decreases with increasing ice content (Are, 1983; Lawson, 1983). Melting ice may also lead to saturation in fine grained, poorly drained thawed sediments, triggering their flow and collapse in a process commonly referred to as thermal denudation

(Kanevskiy et al., 2016) (Figure 1d). Subaerial frozen bank sediments exposed by ice melt water and/or surface runoff can continue to thaw and retreat independent of fluvial erosion (Kanevskiy et al., 2016; Lawson, 1983; Shur et al., 2021; Stettner et al., 2018). Douglas et al. (2023) argued that sediment entrainment and slump-block erosion could control riverbank erosion rates in some cases, rather than pore-ice thaw.

Studies of individual rivers have reached conflicting conclusions regarding the relative influence of permafrost on riverbank erosion rates (Are, 1983; Cooper & Hollingshead, 1973; Leffingwell, 1919). On the Tanana River, AK, Gatto (1984) could not find a clear relationship between local permafrost occurrence and erosion rates. Lena River island head retreat rates were 50%–100% lower where permafrost was present until increases in the combined temperature and discharge of the river led to periods of equal or greater (40%) erosion on these islands (Gautier et al., 2021).

Complicating the attribution of permafrost influence on erosion rates are other regional drivers with the potential to systematically affect bank erosion: climate, hydrology, sediment loading, and river ice. Hydrologically, northern rivers exhibit highly seasonal discharge with peak flows associated with snowmelt runoff (nival) occurring over a few weeks in late spring to early summer, and very limited to no flows (for smaller streams) during winter when covered by ice (Holmes, Coe, et al., 2012; Lafrenière & Lamoureux, 2019; Woo et al., 2008). Low sediment loads may also influence erosion rates; outside the Arctic, sediment loading has been suggested to have a strong positive influence on bank erosion rates (Bufe et al., 2016; Constantine et al., 2014; Dietrich, 1999; Donovan et al., 2021; Dunne et al., 1981, 2010; Torres et al., 2017; Wickert et al., 2013), although other studies argue that locally, high sediment loads may be the result of high bank erosion rates and not a driver (Dingle et al., 2020). Recently, global analysis rates of river mobility, measured by changes in water location, found no correlation between river mobility rates and modeled sediment fluxes (Langhorst & Pavelsky, 2023).

Ice is also a distinctive characteristic of northern rivers. The annual break up of winter ice on high-latitude rivers plays a major role in flooding (Prowse & Beltaos, 2002) and has also been observed to cause localized bank erosion and destruction of riparian vegetation (Boucher et al., 2009; Ettema, 2002; Gautier et al., 2021; Prowse & Culp, 2003; Scrimgeour et al., 1994) (Figure 1e). Studies of small rivers on the north slope of Alaska have documented localized widening of river channels in response to the transitions from bedfast to floating ice in channels (Best et al., 2005; Boucher et al., 2009; McNamara & Kane, 2009; Wohl & Scamardo, 2022). At reach- to watershed-scale, however, the effect of ice on bank erosion remains uncertain with studies concluding that ice has minimal influence (Eardley, 1938; Williams, 1952, 1955), to ice protecting banks (Costard et al., 2014; Miles, 1976; Prowse & Culp, 2003), to ice increasing bank erosion (Best et al., 2005; Brown et al., 2020; Chassiot et al., 2020; Prowse & Culp, 2003; Vandermause et al., 2021) while other studies suggest the available data are inconclusive (Ettema, 2002).

The potential direct and indirect effects of Arctic climate change on riverbank erosion remains uncertain. Lininger and Wohl (2019) hypothesized that increased river discharges and loss of permafrost would accelerate erosion rates; however, they also noted that the possible influx of sediment from rapidly eroding permafrost landscapes could outpace river transport capacities that would in turn drive aggradation of river channels and lead to net bank accretion. Tananaev and Lotsari (2022) concluded that increased water temperatures, flooding, and sediment loads would most likely drive an increase in riverbank erosion, but that floodplain subsidence could decrease erosion rates. On the Lena River, increases in decadal island head erosion rates were correlated with river temperature increases (Costard & Gautier, 2007; Gautier et al., 2021). Using below-bankfull water masks of large sub-Arctic rivers and low flow thalwegs of multi-threaded Arctic rivers, a recent study found a statistically significant but marginal reduction in bank erosion rates over the past 50 years and speculated that the trend may be related to observed greening of northern riparian zones and/or hypothesized changes in shallow groundwater flow (Ielpi et al., 2023).

3. Data Collection and Methods

3.1. Global and Pan-Arctic Analysis

3.1.1. Global Compilation of Published Erosion Rates and Watershed Characteristics

To compare erosion rates measured in watersheds with permafrost to ones without permafrost, we compiled 993 measurements of riverbank erosion from 336 rivers and streams from 169 published English language studies

(Figure 2a) (Rowland & Schwenk, 2019) https://data.ess-dive.lbl.gov/view/doi:10.15485/1571181. For the purposes of this study rivers below 60° north latitude were considered uninfluenced by permafrost, conversely those above 60° north latitude were classified as having permafrost influence. Drainage areas ranged from 0.15 to 3,000,000 km^2 and spanned rivers with widths of 1 m–13 km. The data set included rivers in 17 of the 30 Köppen-Geiger climate zones (Beck et al., 2018). Previously published studies of erosion rates in permafrost regions comprised 9% of the studies in our global compilation.

Channel width, river drainage area, and sediment load and/or yield were recorded if provided in a published study; otherwise, we assembled these ancillary data from other published studies, global and regional data sets, or measured representative widths from Google Earth images (Rowland & Schwenk, 2019) https://data.ess-dive.lbl.gov/view/doi:10.15485/1571181. For reach-based measurements of bankfull width, we used the Lin et al. (2020) data set where available. We used sediment load data from the Land2Sea (L2S) (Peucker-Ehrenbrink, 2009) data set for many rivers where that information was not available elsewhere. We used three data sources for river slopes. First, we used published values of river slopes when reported for the same river reach as the erosion measurements. Second, where available, we used the reported slopes from the global data set of Lin et al. (2020). Finally, we used the rabpro software (Schwenk et al., 2022) https://doi.org/10.21105/joss.04237 to calculate slope along reaches where data were unavailable from the other data sources. The errors associated with slope estimates are discussed in Supporting Information S1 (Text S2). If unique values for width, drainage area, discharge, and slope were not available for individual erosion rates from the same river, we averaged the erosion rates to provide a single value for each set of river characteristics. This averaging reduced the data set to 585 measurements for non-permafrost rivers and 36 for published studies of permafrost rivers.

We classified published erosion rates into two categories based on the spatial scale over which the measurements were made: local, such as at an individual bend, and reach. We then only used the reach-scale measurements to compare our new measurements of erosion rates in permafrost systems. Errors were rarely reported in previous published studies; therefore, we assigned a standard error (SE) of the mean erosion rate of 2% based on the average SE quantified for our permafrost river data set.

3.1.2. Pan-Arctic Satellite and Aerial Photo Analysis

We generated a new data set of riverbank erosion rates across the northern high-latitudes (≥60°N) on 13 Arctic and sub-Arctic rivers with varying permafrost conditions, sizes, and morphologies (Rowland & Stauffer, 2019b) https://data.ess-dive.lbl.gov/datasets/doi:10.15485/1571527. The rivers included the Yukon, Selawik, Koyukuk, Noatak, and Colville Rivers in Alaska, and the Indigirka, Kolyma, Lena, Ob, Pechora, Taz, Yana, and Yenisei Rivers in Russia (Figure 2b). We supplemented our analysis with river masks generated by Brown et al. (2020) for the lower Yukon, Tanana, and Chandalar Rivers in Alaska. The drainage area of the analyzed rivers ranged between 1,300 km^2 (Selawik) and 2.5×10^6 km^2 (Yenisei); widths ranged between 65 m (Selawik) and 6,500 m (Lena); and planform morphologies varied from single-threaded meandering to multi-threaded braided and anastomosing. All river sections analyzed were bounded by alluvial floodplains. Based on published maps of permafrost distributions, all rivers we analyzed have some degree of permafrost in their watersheds and along the river channels (Brown et al., 2002; Gruber, 2012; Obu et al., 2018, 2019; Pastick et al., 2014, 2015) (Figure 2b).

We used 129 images from the Landsat archive, higher resolution satellite imagery, and aerial photography collected between the 1970s and 2018 to generate binary masks of more than 5,500 km rivers in permafrost regions (Table S1 in Supporting Information S1) (Rowland & Stauffer, 2019a) https://data.ess-dive.lbl.gov/datasets/doi:10.15485/1571525. Masks were generated using the automated feature extraction software GeniePro (Perkins et al., 2005) and eCognition (Flanders et al., 2003). Masks of the bankfull channel extent were generated by classifying both water and baer, vegetation-free sediment along the banks and channel islands as part of the active channel (Donovan et al., 2019; Rowland et al., 2016 and references therein). Bankfull channel extent avoids errors associated with using channel masks generated from the visible extent of water alone, which varies with river stage and movement of unvegetated bars and islands. The masks were analyzed using the Spatially Continuous Riverbank Erosion and Accretion Measurements (SCREAM) software (Rowland et al., 2016). A detailed description of both the SCREAM methodology for measuring erosion rates and channel widths may be found in Rowland et al. (2016). All masks were manually inspected and corrected for errors generated by shadows, clouds, and poor classifications prior to analysis with SCREAM.

The accuracy and comparability of SCREAM generated erosion rates to results derived from other published methodology, used to measure erosion rates on non-Arctic rivers, were presented in Rowland et al. (2016). In

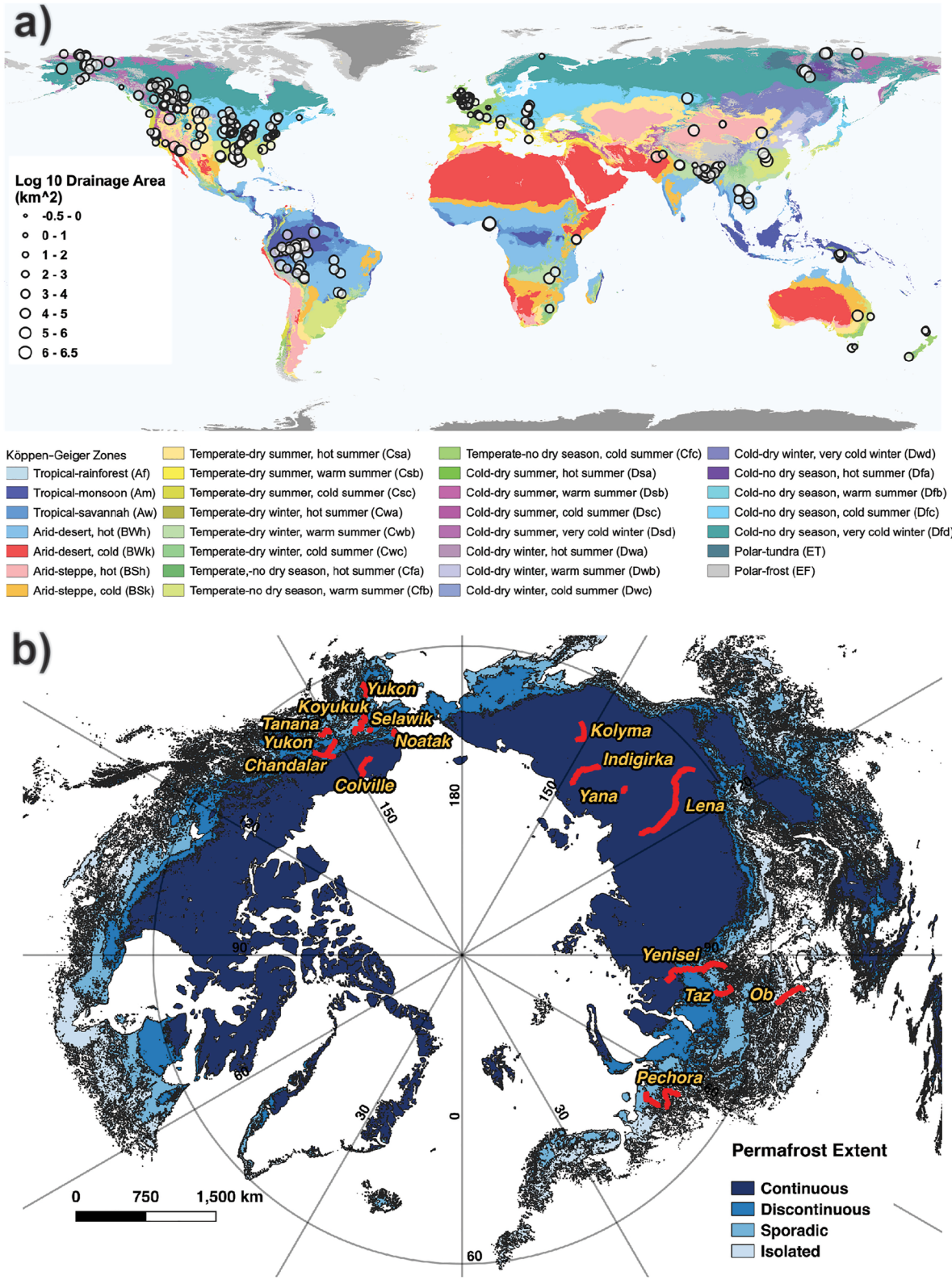

Figure 2. (a) Locations of erosion rates compiled from published studies (Rowland & Schwenk, 2019) https://data.ess-dive.lbl.gov/view/doi:10.15485/1571181. Circle size is logarithmically (base 10) scaled to the upstream drainage area. The underlying map is colored by the Köppen-Geiger climate zone (Beck et al., 2018). (b) Map of rivers permafrost regions analyzed and permafrost extent. Locations of rivers analyzed for bank erosion rates are shown in red. The permafrost map shows zones of permafrost extent from isolated to continuous (Obu et al., 2019 version 2.0).

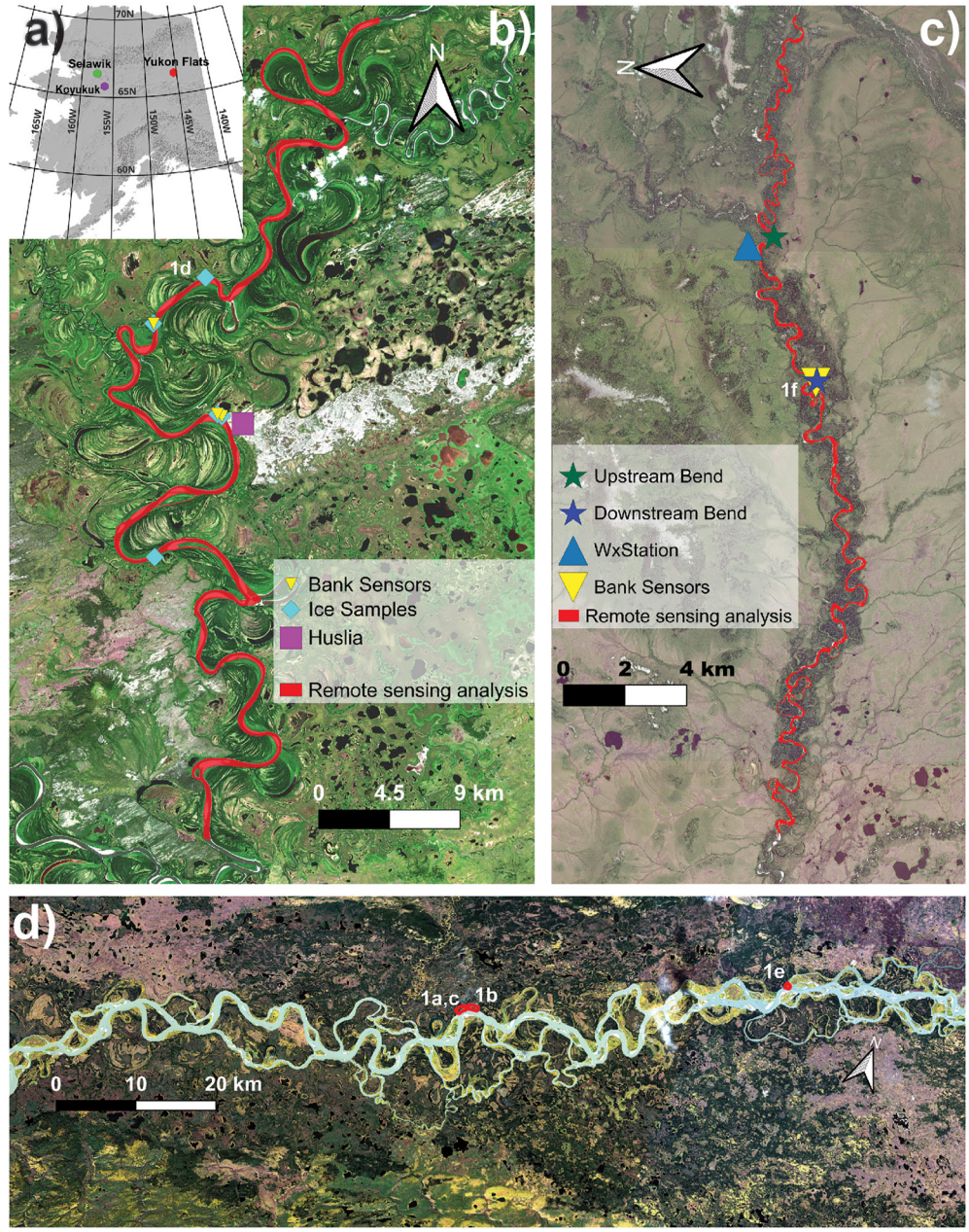

Figure 3. Field study locations. (a) Locations of three rivers where field observations were collected. (b) Koyukuk River with measurement locations highlighted. Background image is a Sentinel 2 scene acquired in July 2022. The river flow is from north to south. Location of image in Figure 1d annotated. (c) Selawik River study reach with locations of sensors and bends discussed in text highlighted. Background is a 2 August 2022 Worldview3 image (©2022 Maxar). The river flows from east to west. Location of image in Figure 1f annotated. (d) Section of the Yukon River in the Yukon Flats where field observations were made in 2009. Red outlines with labels indicate the location of images in Figure 1. Remote sensing analysis includes this entire reach and extends both up- and downstream. Background image is a Sentinel 2 scene acquired in July 2022.

addition, we used SCREAM to measure the erosion rates for three lower latitude rivers (the Ucayali River, Peru, the Strickland River, Papua New Guinea, and the East River, Colorado) that span a broad range of drainage areas. The results of these measurements are both consistent with the published data for these rivers (Aalto et al., 2008; Schwenk et al., 2017) and do not show a bias compared to the complete non-permafrost data set.

We averaged individual bank measurements along sections of rivers to compare reach scale rates to watershed properties, such as drainage area, sediment yield, discharge, slope, and permafrost, and to weight measurements

between rivers proportionately. We created bins based on changes in upstream drainage area, such that the drainage area associated with each new river segment increased by 20% on average with a minimum increase of 5%. For rivers which had multiple time periods of analyses, such as the Yukon, Lena, Koyukuk, and Noatak Rivers, we used only the longest time interval in our global comparison, resulting in a data set of 78 measurements.

Errors in individual measurements of erosion rates and channel width were quantified in Rowland et al. (2016). The largest source of error comes from the ability to accurately classify the location of a riverbank in remotely sensed imagery. Rowland et al. (2016) estimated that the error in bank erosion measurements for any time interval, due to bank classification, was 0.35 pixels. Therefore, the shorter the time interval over which change is measured, the greater the error in erosion rates. In this study, we used the SE of the mean based on the reach-averaging discussed above, which incorporates the measurement uncertainty into the reach-scale measurements.

Donovan et al. (2019) provided an in-depth evaluation of the importance of and methods for incorporating detection limits into the reporting of remotely sensed river migration rates. Here, we assigned a value of zero to all erosion measurements below the threshold of detection. We confirmed that this approach did not lead to image resolution dependent results by comparing rates measured with 30m Landsat imagery to rates measured with high-resolution imagery over approximately the same time intervals (Text S3 and Figure S4 in Supporting Information S1).

To assess other sources of error and bias in our data set, we tested the influence of river planform morphology and measurement time interval on erosion rates (Donovan & Belmont, 2019 and references therein). The hypothesis that the erosion measurements from single- and multi-threaded rivers come from the same distributions could not be rejected using two-tailed Wilcoxon rank sum tests for either permafrost or non-permafrost rivers (Figure S5 in Supporting Information S1). Moreover, there was not a statistically significant correlation between erosion rates and measurement time intervals or length of river segment analyzed in either of our data sets (Figures S6 and S7 in Supporting Information S1).

3.1.3. Analysis of Remotely Sensed and Published Erosion Rates

We conducted two comparisons of permafrost and non-permafrost erosion rates. First, we normalized all erosion rates by bankfull channel width to control for the general trend of increasing erosion rates with river size (Hooke, 1980; Ielpi & Lapôtre, 2020; Krasnoshchekov, 2009; Van De Wiel, 2003). Erosion rates on rivers influenced by permafrost generated in this study were normalized by the local width of the channel at the location where the erosion rate was measured. These normalized rates were then averaged over the longer river segments. The measurements were compared across the full data sets, and separately by reach averaged and locally based erosion rates. The Wilcoxon rank sum test between the data sets was performed with a significance threshold set at 0.05.

Second, we compared permafrost and non-permafrost erosion rates by examining the relationships between erosion rate and stream power (Ω):

$$\Omega = \gamma Q S, \tag{1}$$

where, γ is the specific weight of water (the density of water (ρ) times gravity (g)), Q is the discharge, and S is the river slope. Prior studies have found stream power to be an effective predictor of bank erosion (Akhtar et al., 2011; Bizzi & Lerner, 2015; Hickin & Nanson, 1984; Larsen et al., 2006; Lawler et al., 1999; Moody, 2022; Nanson & Hickin, 1986). Stream power incorporates both hydrological variability through discharge and basin characteristics through slope.

The selection of an appropriate value for Q (Equation 1) requires determining what discharge values are both relevant to bank erosion and comparable across rivers. Numerous studies have shown that the onset of bank erosion correlates to a critical value of boundary shear stress and hence discharge (Darby et al., 2010; Francalanci et al., 2020; Leyland et al., 2015; Rinaldi & Darby, 2007; Rinaldi et al., 2008). This threshold value is often associated with a bankfull discharge, which is commonly assigned based on flow frequency analysis and a specific return interval (Bizzi & Lerner, 2015; Naito & Parker, 2019). Recent modeling suggests that a range of high but not extreme flows may provide a more meaningful hydrological predictor for channel dynamics (Naito & Parker, 2019, 2020).

Few bank erosion studies reported bankfull or maximum discharges, and many of the rivers in both our Arctic and meta-analysis of published erosion rates are ungauged or lack reliable stream flow data for the reaches of interest.

Therefore, we extracted the long-term average (1960–2015) of the FLO1K annual maximum monthly discharge (Barbarossa et al., 2018) using the Python package rabpro (Schwenk et al., 2022) https://doi.org/10.21105/joss.04237. The annual maximum monthly discharge captures both geomorphically relevant discharges that occur for sufficient durations to be effective and avoids biases of short-lived outliers potentially captured in the annual maximum daily discharge.

In our regression analysis of erosion rates, we sought to address two potential sources of uncertainty and bias. First, our data sets have non-uniform errors in erosion rates, and second, our measurements were not uniformly distributed across stream power, raising the possibility that linear regressions to the data sets could be influenced by outliers. To address these issues, we used a bootstrap method for regression. We randomly sampled with replacement 5,000 subsets of the original stream power—erosion rate data pairs. Each of the 5,000 subsets was the same length as the two original data sets (permafrost and non-permafrost). For each randomly selected stream power value an erosion rate was randomly selected from a normal distribution of erosion rates constructed from the mean erosion rate and a standard deviation equal to the SE of the mean erosion rate. We then log10-transformed both the randomly selected stream power and erosion rate values and fit a linear regression to the transformed data. From the 5,000 regressions, we obtained a distribution of mean slopes, intercepts, r^2, *p-values*, and values corresponding to the 95th confidence intervals that incorporate the uncertainty in erosion rate measurements and test the possible influence of outliers. The influence of outliers was minimized because no single sample retained all the original values in the data set. On average, 63% of the original stream power-erosion pairs were included in any individual sample, the maximum percentage of the data set in any sample was 70%.

3.1.4. Analysis of the Influence of River Hydrology and Sediment Load

To test alternative hypotheses that hydrology could explain differences in erosion rates between permafrost influenced and permafrost free rivers, we used global hydrological databases of river discharges L2S (Peucker-Ehrenbrink, 2009) and the Dai and Trenberth (Dai & Trenberth, 2002). We evaluated whether strong seasonality of peak river flows leads to relatively inefficient bank erosion due to the potential non-linear (<1) relationship between river discharge and shear stresses driving bank erosion such that greater time-integrated erosion rates for the same total annual discharge may be possible under differing hydrographs. We modeled erosion rates along the Yukon and Lena Rivers by redistributing the total annual flows for the Yukon and Lena River based on the hydrographs of nine lower-latitude rivers that spanned seven climate zones and had stream powers ranging from 1,400 to 4,000 W m^{-1}. This analysis was performed with multi-year averages of daily discharges to generate representative hydrographs (Text S5 in Supporting Information S1).

We used a widely applied excess boundary shear stress model of bank erosion that does not attempt to account for bend specific hydrodynamic controls on erosion rates (Darby et al., 2007; Francalanci et al., 2020; Midgley et al., 2012; Partheniades, 1965; Pizzuto, 2009; Zhao et al., 2022):

$$E = \kappa_d(\tau_b - \tau_c)^{\alpha} \quad (2)$$

where E is the linear erosion per unit time, κ_d is an erodibility coefficient with units of $m^3/N/s$, τ_b and τ_c are the boundary and critical shear stress for the initiation of bank erosion in Pa, respectively, and α is a dimensionless exponent commonly set to 1 (Rinaldi et al., 2008; Zhao et al., 2022). Parameterization of Equation 2 and data sources for the Yukon and Lena Rivers are presented in Supporting Information S1 (Text S5).

3.2. Field Observations and Measurements

We conducted field investigations along two rivers (Yukon and Koyukuk) in the boreal forest region of Alaska (Young et al., 2017) and one river (Selawik) in tussock tundra dominated western Alaska (Raynolds et al., 2019).

3.2.1. Koyukuk River, Alaska

We conducted field work on the Koyukuk River near the Village of Huslia (65.7 N, 156.4 W) in 2018. This section of the Koyukuk River flows through an extensive floodplain up to 18 km wide that is located south of the Brooks Range and north of the river's confluence with the Yukon River. The Koyukuk drains 80,000 km^2 upstream of the study reach. The mean annual discharge at the Hughes gauging station (66.0475°N, 154.258°W) located just upstream of the study reach averaged 406 m^3/s between 1961 and 1981 (https://waterdata.usgs.gov/nwis/inventory/?site_no=15564900). Along this section, the Koyukuk is primarily a single-threaded and meandering sand bed

river. The floodplain is composed of sandy deposits overlain by silty fines with scroll bar complexes easily visible due to the coincidence of curvilinear rows of trees. At the village of Huslia, a site of pronounced local erosion in permafrost-free aeolian bluffs, residents have reported average riverbank erosion rates of 3–9 m/yr, with a yearly maximum of 30 m in 2004 and episodic rates of erosion as high as 18 m in a single spring flood in 2003 (U.S. Army Corps of Engineers, 2007).

Vegetation on the floodplain is heterogeneous with willow in early successional areas along the river, such as point bars and older portions of the floodplain are covered by a mix of black spruce, white spruce, and aspens. Treeless expanses of old oxbows and drained lakes are covered by grasses and generally lack permafrost. Mosses and tundra vegetation overlay older deposits with permafrost. Both field observations and published maps (Obu et al., 2019; Pastick et al., 2015) indicate that the floodplain is underlain by discontinuous permafrost with strong correlations between vegetation cover and the presence of near surface permafrost. Ice content in frozen sediments is highly variable, with excess ground ice commonly observed in drained lake basins. Based on the Climatic Research Unit 0.5° data, the mean annual temperature at Huslia was −5.3°C between 1978 and 2018, with a 0.03°/yr increase in mean annual temperature over that time period (Harris et al., 2020).

Field work on the Koyukuk River was conducted in June and July of 2018. Surveys to determine the location and extent of permafrost consisted of coring, digging pits, trenching of cutbank faces, and a visual inspection of banks from a boat to note distinctive permafrost features (e.g., overhanging tundra mats, thermoerosional niching, ice wedges, active drainage of ice melt from soils). Coring locations were chosen based on where permafrost was suspected to be present or absent and to sample a range of geomorphic units and relative deposit ages based on scroll bar and meander patterns preserved on the floodplain. Coring was conducted using a Snow, Ice, and Permafrost Research Establishment corer, designed to core into frozen soils. Cores were 1–2 m in length and the presence of permafrost was inferred by the existence of frozen soil at depth. We also conducted more extensive permafrost surveys using a soil probe to note the presence or absence of frozen ground in the upper 1 m of soil (the length of the probe). These observations and multispectral WorldView 3 imagery acquired in May 2018 and interferometric synthetic aperture radar data were used to train a convolutional neural network model (CNN) to predict the occurrence of permafrost across the study site (Schwenk et al., 2023) https://data.ess-dive.lbl.gov/datasets/doi:10.15485/1922517.

At exposed bank faces, thawed sediment was removed, and the underlying frozen bank was inspected to characterize grain size, stratigraphy, and ice structures. A concrete corer 210 ml in volume was used to extract frozen samples from the exposed bank face at 11 locations across five banks to measure bulk density and ice content. We used the *pvlib* python package (Holmgren et al., 2018) to calculate the average annual total direct solar irradiance at each of these five riverbanks. Riverbank temperatures were monitored at five locations along 3 riverbanks using an array of iButton loggers installed in a custom rod manufactured by Alpha Mach Inc. The temperature loggers were located at the bank face, 5, 10, 20, and 40 cm depths (Rowland et al., 2023) https://data.ess-dive.lbl.gov/datasets/doi:10.15485/1922885.

3.2.2. Selawik River, Alaska

The Selawik River flows east to west on the southern side of the Kiliovilik Range on the southern margin of the Brooks Range. Field research was conducted in the vicinity of an actively eroding retrogressive thaw slump (Barnhart & Crosby, 2013) near the confluence with the Kiliovilik Creek, Alaska (66.49°N, −157.60°W) in 2010, 2011, and 2012. Along the study reach the drainage area ranges from 1,100 to 2,000 km^2 and the average channel width is 65 m. The largely single-threaded river has a gravel bed with filled and partially filled abandoned channel segments occupying a floodplain approximately 1 km in width. The Selawik River is ungauged but modeled river discharges estimate a long-term mean annual discharge of 27 m^3/s (Barbarossa et al., 2018).

The region is characterized by shrubby tussock tundra with birch and willows along river and stream corridors (Cable et al., 2016; Jorgenson et al., 2009). Mean annual air and 1 m deep soil temperatures near our study sites were reported as −4.6 and −3.9°C, respectively (Cable et al., 2016). Though mapped at the transition between discontinuous and sporadic permafrost zones (Obu et al., 2019; Pastick et al., 2015), we observed permafrost to be present along most of the floodplain except for active and newly abandoned point bar deposits and gravel-dominated channel fills with overlying silt deposits less than 40 cm thick. Observations of excess ground ice were limited to isolated ice wedges exposed in eroding hillslopes and lowland surfaces topographically above the present-day floodplain.

Soil and air temperatures on the Selawik were recorded at hourly time intervals (Rowland et al., 2023) https://data.ess-dive.lbl.gov/datasets/doi:10.15485/1922885. Soil temperature sensors were placed 50 cm below the ground surface at 66.48°N, 157.71°W. Air temperatures were recorded two m above the ground surface at a weather station located 5 km upstream (66.500°N, 157.609°W).

3.2.3. Yukon River, Alaska

We conducted field work in the Yukon Flats of central Alaska near the Village of Beaver (66.3594°N, 147.3964°W) in the summer of 2009. This reach has been classified as a wandering planform morphology (Clement, 1999) and features multiple threads with a few dominant channels and large stable islands. An upstream drainage area of 500,000 km^2 generates a mean annual discharge of 3,450 m^3/s measured at the stream gauge located at the downstream end of the study reach (https://waterdata.usgs.gov/nwis/inventory/?site_no=15453500). In this section of the river, the total width varies from 1,500 to 2,700 m. The bed material is dominated by gravel. Riverbanks ranging in height from 4 to 6 m are composed of gravel in the lower half and overlain by sandy overbank deposits, and a reported slope of 0.0001 (Clement, 1999).

4. Results

In the following sections, we present results from the largest spatial (pan-Arctic and global) and temporal (decades) scales and progressively decrease in magnitude to examine riverbank erosion at the smallest spatial (riverbank) and temporal (days) scales.

4.1. Pan-Arctic Erosion Rates Relative to Non-Permafrost Rivers Systems

Rivers with permafrost showed a clear and statistically significant difference in bankfull width-normalized erosion rates relative to rates measured in permafrost-free watersheds (Figure 4a; two-tailed Wilcoxon rank sum tests ($p\text{-value} < 0.001$)). Erosion rates grouped by reach scale measurements indicated that permafrost-influenced rivers had normalized erosion rates 9 times lower (0.006 ± 0.001 vs. 0.053 ± 0.012, mean $\pm$ SE). Grouped across all measurements and for local scale measurements, permafrost rivers also had mean-normalized erosion rates with statistically significant lower rates.

The non-normalized reach-scale bank erosion rates for both permafrost and non-permafrost rivers showed a correlation with the estimated stream power for each river reach (Figure 4b). The mean best fit regression yielded statistically significant ($p\text{-value} < 0.01$) power law relationships for both sets of riverbank erosion rates: non-permafrost $E = 0.008(+0.014, -0.005)\Omega^{0.77(+0.85, -0.68)}$; permafrost $E = 0.19(+0.36, -0.09)\Omega^{0.23(+0.31, -0.16)}$ (the numbers in parentheses are the values of the upper and lower 95th confidence intervals). Stream power proved to be a stronger predictor of bank erosion rates in non-permafrost ($r^2 = 0.58$) than permafrost ($r^2 = 0.27$) rivers. None of the 5,000 bootstrapped regressions yielded slopes for either data set that overlapped with the other.

None of the permafrost rivers for which we measured erosion rates had stream powers lower than the point of intersection of the two regression lines ($\Omega \sim 350$ W m^{-1}). We plotted the four lowest stream power data points (diamonds) in the data set of the previously published rates (all based on local studies). Two locations fall above the intersection of regression lines and two below; the ones below plot on the same regression line as the non-permafrost data set. We also marked (black triangles) three non-permafrost rivers we analyzed with the SCREAM methodology to highlight that the trend of our permafrost data set does not appear to be an artifact of the analysis method.

A pan-Arctic comparison of the location of erosion rate measurements with published maps of permafrost (Brown et al., 2002; Gruber, 2012; Obu et al., 2018, 2019) does not show a correlation between erosion rates and the relative extent of permafrost in the basin or individual river reaches. Our evaluation of these permafrost products (Text S6 in Supporting Information S1) showed high uncertainties regionally, particularly in areas of variable permafrost such as floodplains. For example, in the Yukon Flats region of Alaska, a local permafrost map and a statewide data product produced by the same research group had significant disagreement at the scale of individual river reaches and bends (Pastick et al., 2014, 2015). Therefore, at the pan-Arctic scale, we can only conclude that rivers with some extent of permafrost have lower reach-averaged bank erosion rates compared to rivers with equivalent stream power in basins without permafrost. The difference in erosion rate is up to 40 times at stream powers of 400,000 W m^{-1} but becomes insignificant at stream powers less than 1,000 W m^{-1}.

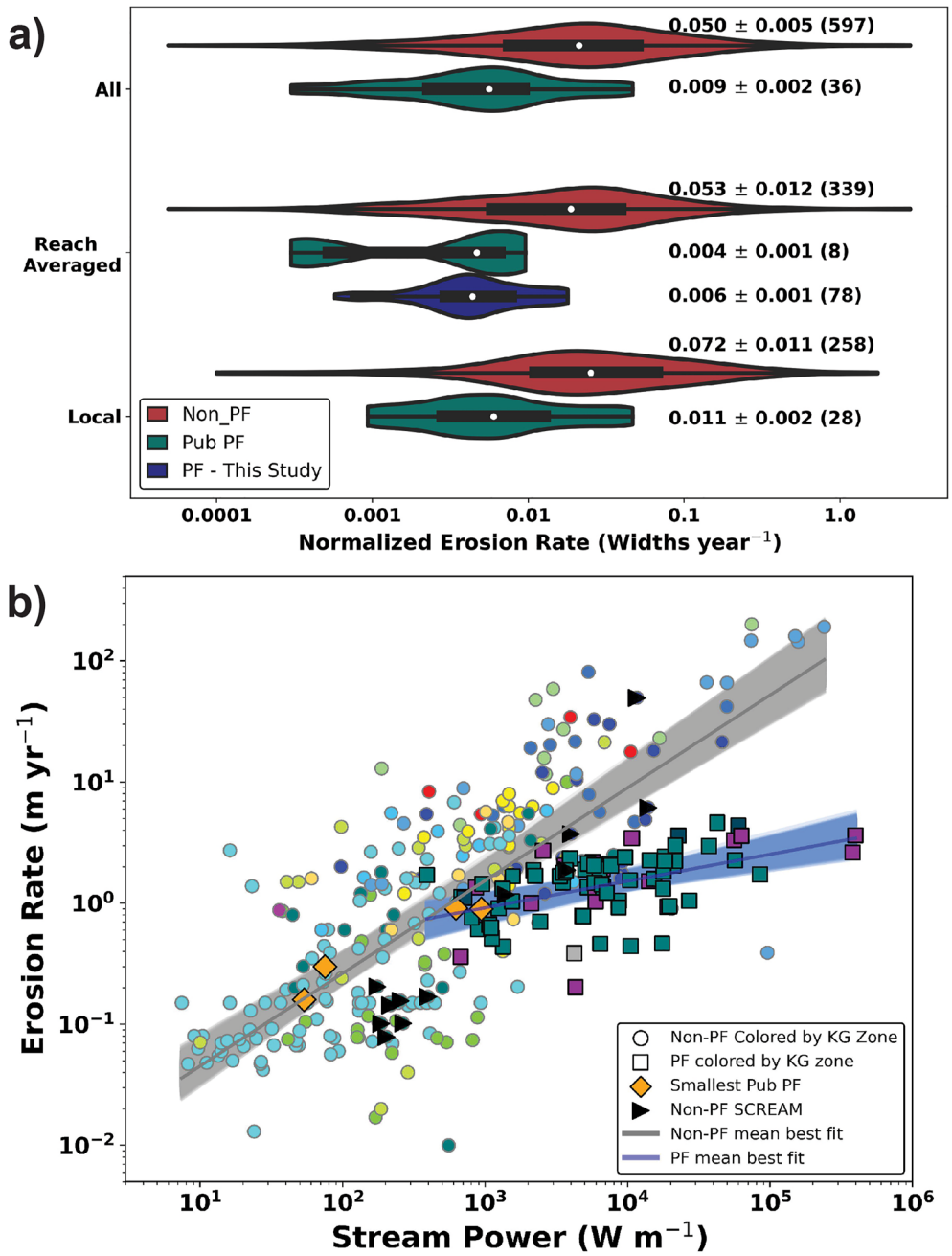

Figure 4. Comparisons of permafrost and non-permafrost riverbank erosion rates. (a) Violin plots of width-normalized riverbank erosion rates for permafrost and non-permafrost rivers. These plots show the range and distribution of bank erosion rates from published data and our analyses. The *y*-axis indicates three categories: "All"-data regardless of the scale of measurement, "Reach-averaged" measurements, and "Local" measurements (point to bend-scale). The black rectangles display the interquartile range, the lines indicate the 1.5x interquartile range, white dots represent median values. The numbers report the mean, standard error, and number of observations (in parentheses). (b) Reach-averaged erosion rates plotted by stream power. Circular points are data compiled from published studies and squares are permafrost rivers analyzed in this study. All points are colored by the Köppen-Geiger climate zones (Beck et al., 2018) shown in Figure 2a. The solid gray and blue lines show the mean best fit regressions from the 5,000 bootstrapped linear fits to the log10 transformed data. The shaded regions show all the regressions that fell within the 95th confidence intervals based on the distributions of modeled slopes. Diamond symbols show the published erosion rates of rivers with the smallest stream powers.

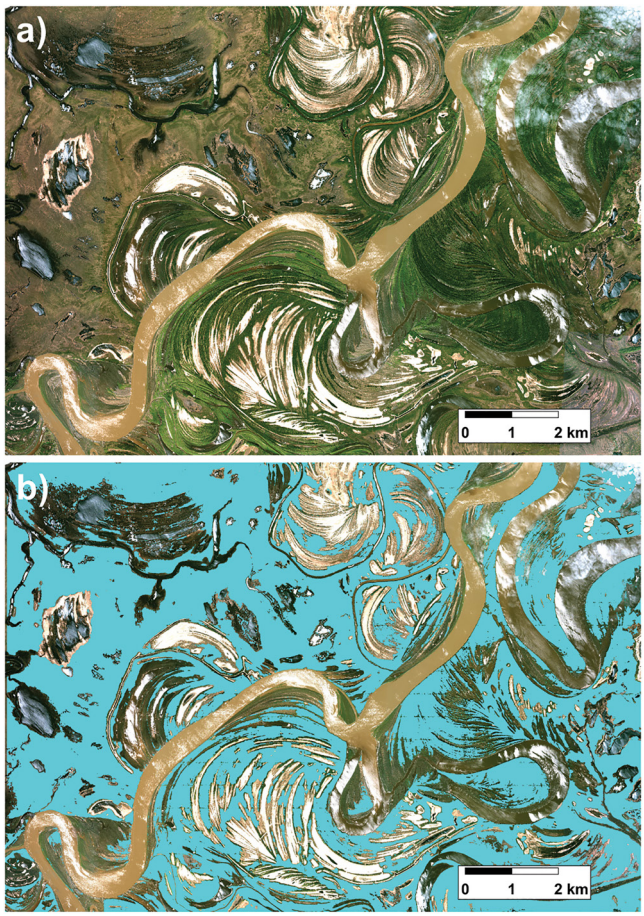

Figure 5. Example segment of permafrost map generated for the Koyukuk River, AK. (a) May 2018 Worldview3 image of the Koyukuk River just upstream of the Village of Huslia (©2018 Maxar). (b) Mapped permafrost extent (blue) of the Koyukuk River floodplain.

4.2. Reach and Bend-Scale Erosion Rate Variations With Permafrost Extent

Using the permafrost map we generated for the Koyukuk River (Section 3.2.1) (Figure 5), we found that erosion rates averaged over 10-channel width long segments showed a general trend in decreasing erosion rates as the fraction of permafrost in the surrounding floodplain increased from 0.23 to 0.72 (Figure 6a). Erosion rates averaged at the individual bend scale (Figure 6b) also showed clear correlation between permafrost extent and decreases in erosion rates.

4.3. Bank Erosion Rates and Volumetric Ice Content

Volumetric ice content at five bends we sampled on the Koyukuk River ranged from 0.41 to 0.76 (Rowland et al., 2023) https://data.ess-dive.lbl.gov/datasets/doi:10.15485/1922885. Erosion rates decreased with increasing ice content at four of the five locations (Figure 6c); the fifth location had the highest ice content and exhibited the highest erosion rates. Of the two locations with the highest ice contents (0.72 and 0.76), the location with the lowest erosion rates faced almost due north (321°) and the one with the highest rates faced almost due south (179°). A comparison of the total annual irradiance to erosion rates and ice content (Figure 6c righthand vertical axis) showed that the rapidly eroding, high-ice content, south-facing bank received approximately three times as much direct solar radiation as the north-facing, high ice content bank. The rapidly eroding bank showed clear evidence of thermal denudation in the field with water generated by melting ice, causing active slumping of the fine-grained banks and subaerial retreat (Figure 1d). A comparison of erosion rates to annual direct irradiance at all bends in this section of the Koyukuk River, however, suggests that irradiance alone is not a strong predictor of erosion rates, even in banks with large fractions of permafrost (Figure S9 in Supporting Information S1).

4.4. Riverbank Grain Size and Vegetation Influence on Erosion Rates

Erosion rates measured between 1981 and 2009 along a 45 km reach of the Selawik River averaged 0.68 ± 0.03 m/yr (all rates are the mean and SE) and ranged from 0 to 5.7 m/yr. This range highlights the spatial variability commonly observed across the full permafrost river erosion data set (Rowland & Stauffer, 2019b) https://data.ess-dive.lbl.gov/datasets/doi:10.15485/1571527. To explore controls on this variability, we collected field observations and analyzed 7 years of 2 m resolution satellite imagery at two bends 5 km apart. The bends had equivalent hydrology, similar width-normalized radii of curvature (2.6 vs. 2.7), and both were eroding permafrost-dominated floodplains. Despite these similarities, one bend (shown in Figure 1f) had a 28-year averaged erosion rate of 3.90 ± 0.11 m/yr and the other 0.40 ± 0.07 m/yr (Figure 7a).

Bend-averaged erosion rates between 2009 and 2016 at the rapidly eroding bend ranged from non-detectable to 4.65 ± 0.66 m/yr (Figure 7a). Only two of these years had erosion rates close to or exceeding the longer-term average. Field observations indicate that most of the annual bank erosion occurred in a few days of snowmelt-driven flows during the spring. We observed total erosion of 5.4 m in one section of this bend in the spring of 2011, 63% of which occurred over less than 4 days.

The temperature sensor data from the rapidly eroding riverbank (Rowland et al., 2023) https://data.ess-dive.lbl.gov/datasets/doi:10.15485/1922885 led us to infer that the bank remained frozen until the bank materials collapsed into the river. On 25 May 2011, the temperature sensor originally installed 2 m from the eroding bank face recorded an abrupt increase in temperature from −0.16 to 4°C between hourly measurements and then ceased recording data (Figure 7b). We interpret the jump in temperature to reflect the sensor encountering river water just prior to the sensor being lost. A nearby sensor, initially located 7 m from the bank face, buried at the same depth recorded a ground temperature of −0.9°C, indicating that sediments in the proximity of the bank face remained frozen throughout this time period.

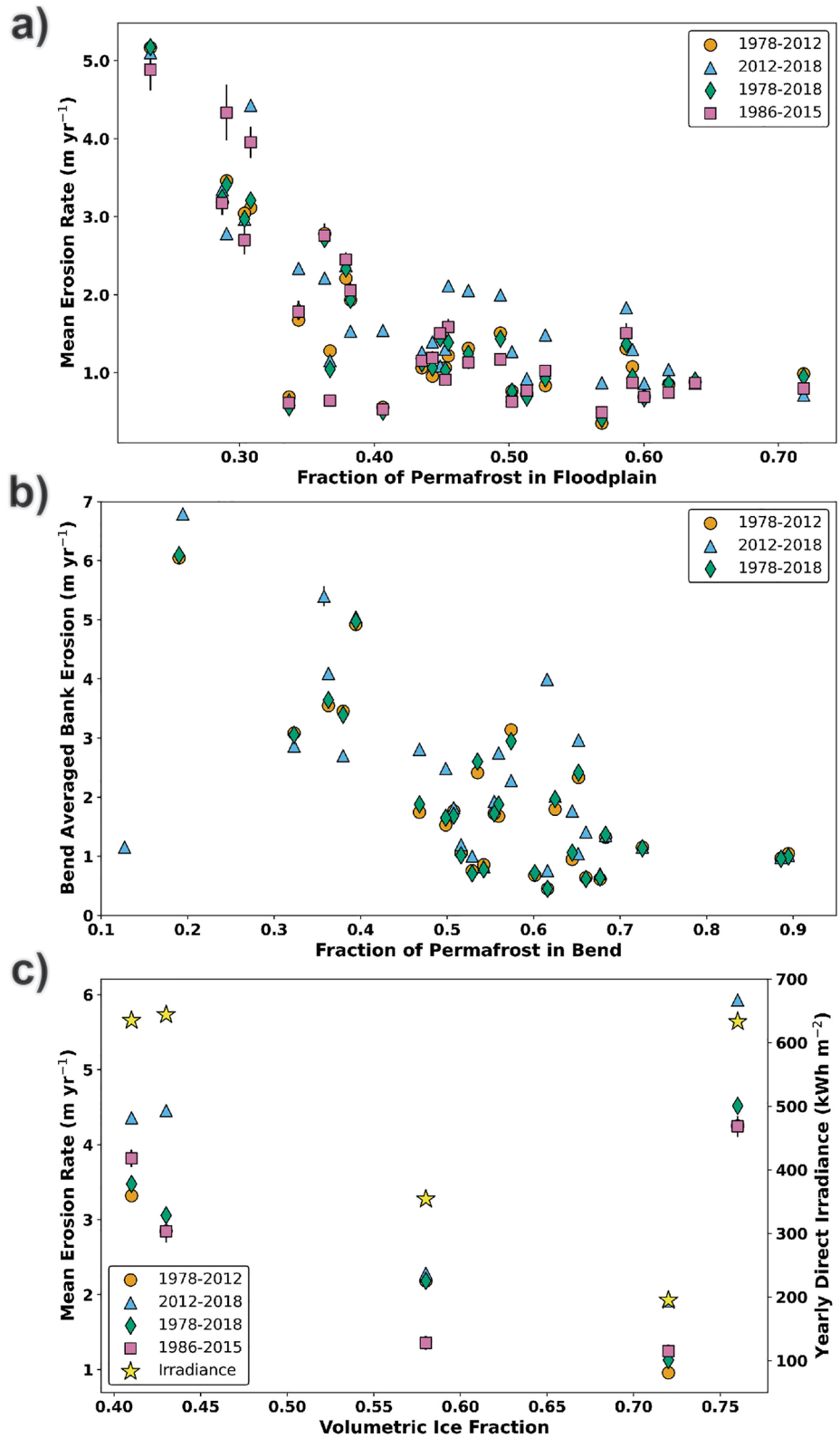

Figure 6.

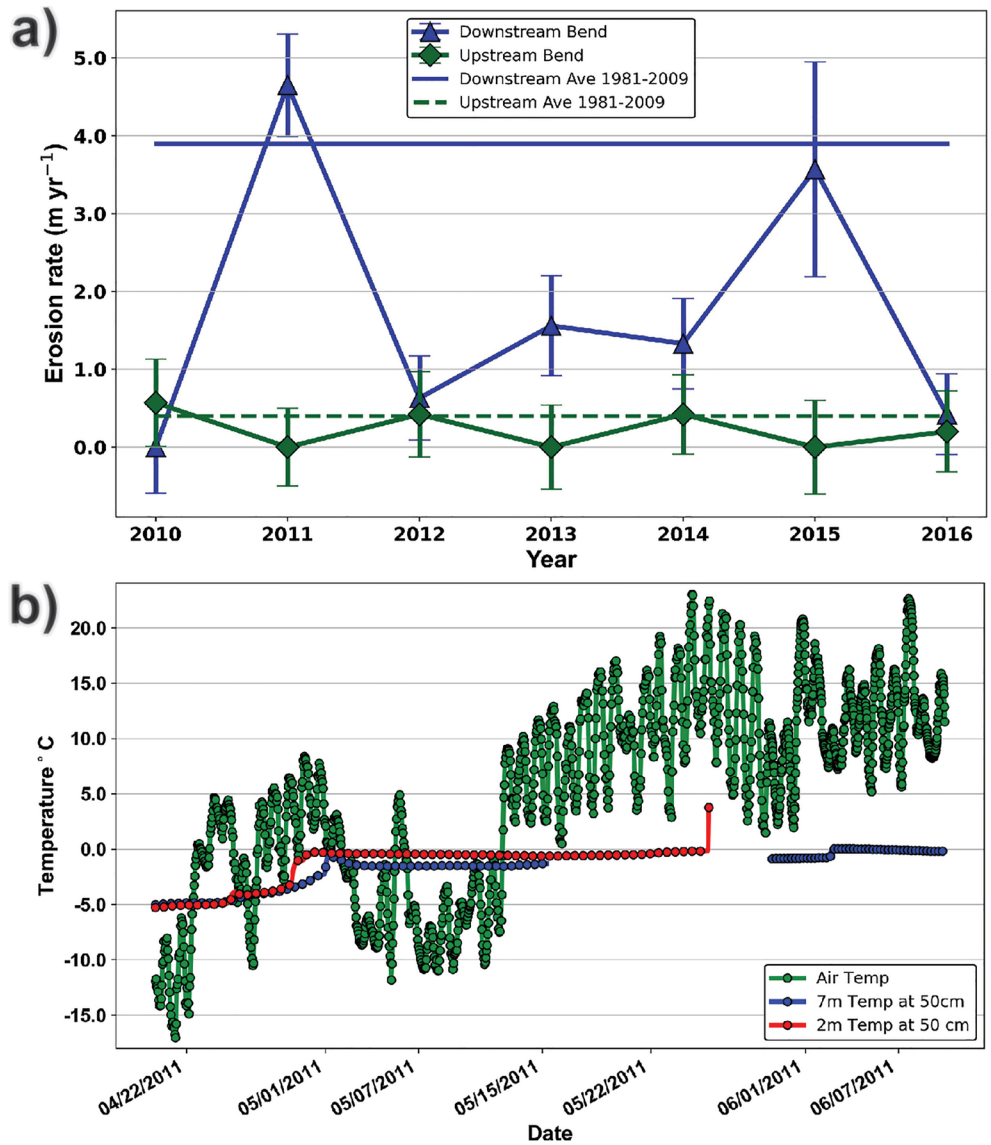

Figure 7. Erosion rates and thermal conditions of riverbanks along the Selawik River, AK. (a) Bend averaged erosion rates for two bends at yearly intervals from 2010 to 2016. Horizontal lines indicate the long-term (1981–2009) erosion rates for each bend. Error bars show the standard error of the erosion rates. (b) Air and riverbank soil temperatures at the downstream river bend shown in (a). Hourly soil temperature data collected at a depth of 50 cm, initially located 2 and 7 m from the riverbank face (the 7 m sensor was 1.6 m from the bank face at the end of May 2011). In May 2011, bank erosion exposed the 2 m temperature sensor (red) to river water prior to the sensor being lost and data collection ending. Plot markers for the soil temperatures are only displayed every 12 hr for visibility. Local air temperatures are plotted in green to highlight the spring warming. Figure 1f shows the downstream bend where the bank temperatures were recorded (panel b).

This bend exhibited little to no erosion during times of lower river discharge throughout the ice-free season despite abundant loose gravels mantling the bank face and toe. During this period, blocks of tussock tundra that had collapsed following high snowmelt flow-driven bank undercutting (Figure 1f) appeared to help protect the

Figure 6. (a) Riverbank erosion rates averaged along segments approximately 10 channel widths in length on the Koyukuk River, AK, plotted against the fraction of permafrost mapped in the surrounding floodplain. Linear regressions were significant at p-values < 0.01 for all time periods; the r^2 values were 0.52, 0.49, 0.51, and 0.50 for 1978–2012, 2012–2018, 1978–2018, and 1986–2015, respectively. (b) Riverbank erosion rates averaged over outer banks on individual bends along the Koyukuk River, AK, plotted against the fraction of permafrost mapped in the surrounding floodplain. Linear regressions were significant at p-values < 0.01 for all time periods; the r^2 values were 0.54, 0.33, and 0.54 for 1978–2012, 2012–2018, and 1978–2018, respectively. (c) Erosion rates of individual riverbank segments (left vertical axis) plotted by the volumetric ice content of bank material and the modeled yearly solar irradiance received by the bank (right vertical axis). In all plots, the vertical lines on the points show the standard errors of the erosion rates, where not visible the SE is smaller than the symbol.

bank from erosion even during late-season rainfall-induced high flows of similar magnitude to snowmelt flow that actively transported bank sediment. Despite their persistence following high summer flows, these blocks were not present following ice-break up in the spring. Similarly, Walker et al., 1987 observed that hanging tundra mats that froze into winter ice tore out during spring breakup. Vandermause et al. (2021) also observed that river ice breakup effectively removes protective vegetation and exposes river banks to new erosion.

Remotely sensed, yearly measurements of bank erosion rates between 2009 and 2016 at the slowly eroding upstream bend ranged from non-detectable to 0.57 ± 0.56 m/yr (Figure 7a). Unlike the gravel dominated, rapidly eroding downstream bend, this bank was composed of fine to medium sand, and tussock tundra covered its face. Our excavation of the bank face revealed that this tundra was associated with failure blocks that had collapsed and refrozen to the underlying sandy deposits. These blocks appeared to remain fixed to the bank throughout the spring ice-out flows and were extremely difficult to remove during bank excavation.

4.5. Subaerial Thaw and Retreat of Riverbanks, and River Ice Driven Erosion

In addition to the thermal degradation of the ice-rich, south facing riverbank on the Koyukuk (Figure 1d), we observed both transient and persistent subaerial thaw and retreat of riverbanks along both the Yukon and Koyukuk Rivers. Along both rivers, frozen bank materials were exposed at the bank face immediately following the recession of high flows and at locations where steep bank geometry prevented the accumulation of thawed sediments (Figure 1a). Following flow recession, subaerially exposed bank sediments appeared to thaw rapidly. On the Koyukuk River, we installed five temperature sensor arrays horizontally at bank locations with high ice contents composed of silty sediments (corresponding to the 0.57 ice content location of Figure 6c), and lower ice content fine to medium sands (two lowest ice content points on Figure 6c). Prior to installing the temperature arrays, we removed all thawed sediment down to frozen materials. Over the course of 2 weeks in the late June and early July 2018, the banks thawed between 40 and 124 mm/day with rates generally decreasing with higher ice contents (Rowland et al., 2023) https://data.ess-dive.lbl.gov/datasets/doi:10.15485/1922885. In all locations, the thawed materials remained in place and created a thermal buffer between the diurnally fluctuating air temperatures and the advancing thaw front. This buffer reduced the thaw rate by 40% between the 0–10 cm and the 10–20 cm distances from the bank face.

Along both the Yukon and Koyukuk Rivers, subaerial portions of the exposed vertical bank faces and the undersides of thaw niches continued to retreat even when not directly exposed to river water. This retreat occurred as thawing chunks of bank material spalled off the subaerial face and dropped into the flowing river and were carried away from the bank face (Figure 1a). Along banks with extensive thermal niches on the Yukon River, massive failure blocks that were 10 m wide and several meters thick were observable in July 2009 (Figure 1b), with similar observations in 2022 by Douglas et al. (2023). Despite their size, the blocks appeared to thaw rapidly, and rarely appear in high-resolution imagery persisting from 1 year to the next. Shallowly rooted trees and tundra tended to detach and slide off the tilted blocks (Figure 1b), offering limited bank protection from further erosion.

In June/July 2009, we observed one additional mechanism for non-fluvial bank erosion on the Yukon River in the Yukon Flats. At a limited number of locations, concentrated at the head of islands, several decimeters of sediment were removed from the floodplain surface during spring ice out, as if scraped off by a bulldozer (Figure 1e). The ice-impacted bank sections appeared spatially limited on the Yukon and potentially had a minimal effect on the lateral retreat of the riverbanks.

5. Discussion

Our pan-Arctic analysis showed that rivers in basins with permafrost on average have width-normalized bank erosion rates nine times lower than non-permafrost rivers (Figure 4a). This rate difference increased with river size and stream power from negligible to 40 times at the highest stream powers (Figure 4b). The results from the Koyukuk River suggest that permafrost concentration has a significant control on variations in bank erosion rates for this river with robust linear decreases in erosion rates as permafrost in the riverbanks increases (Figure 6). With the uncertainty in local accuracy of modeled permafrost occurrence across the Arctic (Text S6 in Supporting Information S1), we do not have clear evidence for similar relationship at the pan-Arctic scale. While across all rivers we see significant variation in the range of erosion rates for given permafrost fractions, we do observe clear upper bounds on the maximum rates of erosion. We interpret these results to indicate that many factors control local bank erosion rates, but permafrost systematically sets an upper limit on these rates.

Our finding is that permafrost exerts a strong control on riverbank erosion. However, prior research has suggested that other characteristics of permafrost-affected rivers may have equal or greater control on riverbank erosion rates than permafrost. Therefore, we examined three possible alternative hypotheses to assess the hypothesis that permafrost is the dominant control of lower erosion rates observed in these river systems.

5.1. Alternative Hypothesis 1: Shorter Annual Flow Durations in Northern Rivers Result in Comparatively Less Flow Relative to Basin Size

Given the short duration over which Arctic rivers flow, these rivers may have less total discharge relative to basin drainage area than comparable non-permafrost rivers. Despite the strong seasonality of discharge in northern high-latitude rivers (Church, 1977; Holmes, Coe, et al., 2012; Woo et al., 2008), a comparison of the total annual discharge versus drainage basin size showed no clear distinction between permafrost and non-permafrost systems (Figure 8a). We analyzed the linear relationship between total annual discharge and drainage basin size using the L2S data set (Peucker-Ehrenbrink, 2009). The paired *t*-test of the slopes (Zar, 1999) indicated that the relationship between total annual discharge and drainage basin size did not differ between permafrost and non-permafrost systems ($p\text{-}value = 0.2$; Figure 8a). The Amazon River was excluded from this analysis because it is a global outlier, even within non-permafrost systems (Milliman & Farnsworth, 2013). The null hypothesis that the specific water yields (annual river discharge divided by drainage basin area) for permafrost and non-permafrost rivers come from the same populations cannot be rejected by a two-tailed *t*-test ($p\text{-}value = 0.9$). An evaluation using the Dai and Trenberth (2002) data sets yielded identical results (Figure S10 in Supporting Information S1). We thus conclude that differences in flow volumes between permafrost and non-permafrost rivers are not likely responsible for the discrepancy in erosion rates.

5.2. Alternative Hypothesis 2: Shorter but Larger Flow Peaks Result in Less Efficient Erosion

The second alternative hypothesis is that the extreme seasonality of peak Arctic river flows leads to relatively inefficient bank erosion due to the potential non-linear (<1) relationship between river discharge and shear stresses driving bank erosion. That is, rivers with flow distributed more evenly in time may have greater time-integrated erosion rates for the same total annual discharge. Using our modeled erosion rates (Section 3.1.4, Figure 8b, Text S5 in Supporting Information S1), we found that in most cases the modeled total erosion using the flatter hydrographs equaled or exceeded the modeled erosion using natural hydrographs for both the Yukon and Lena (Figure 8c). The magnitude of erosion increases (27% maximum), however, failed to explain the 40 times greater erosion rates observed on lower latitude rivers of equivalent drainage areas (Figure 4b); thus, we rejected the second hydrological hypothesis for lower erosion rates for permafrost rivers.

The rejection of alternative hypotheses 1 and 2 suggests that differences in hydrology between rivers in permafrost regions and other river systems are not adequate to singularly explain the regional differences in erosion rates. The power law regressions in Figure 4b also indicated that stream power (hydrology) has much less predictive power for bank erosion in permafrost ($r^2 = 0.27$) than for river systems without permafrost ($r^2 = 0.58$).

5.3. Alternative Hypothesis 3: Lower Sediment Loads in Permafrost Regions Lead to Lower Bank Erosion Rates

Previous studies suggested that riverbank erosion rates increase with a river's sediment load (Constantine et al., 2014; Dietrich, 1999; Dunne et al., 1981, 2010; Torres et al., 2017). This is supported by the positive correlations between sediment loads and rates of lateral channel migration documented along rivers in the Amazon basin (Constantine et al., 2014), and in laboratory experiments (Bufe et al., 2016; Wickert et al., 2013). These observations led us to explore whether the observed differences in erosion rates could be explained by the significantly lower sediment loads measured in permafrost rivers as compared to non-permafrost systems (Gordeev, 2006) (Figure 9a). However, a comparison of erosion rates showed no correlation between width-normalized erosion rates and sediment yield either by permafrost grouping or globally (Figure 9b). We also found no correlation between modeled sediment yields (Cohen et al., 2013) and erosion rates for river reaches in our data sets (Figure S11 in Supporting Information S1). At the global scale, Langhorst and Pavelsky (2023) also found no relationship between river mobility and modeled sediment fluxes.

The absence of a correlation between erosion rate and sediment yields does not rule out that sediment loads may influence riverbank erosion rates. Improved cold region sediment transport models (Zhang et al., 2021) may

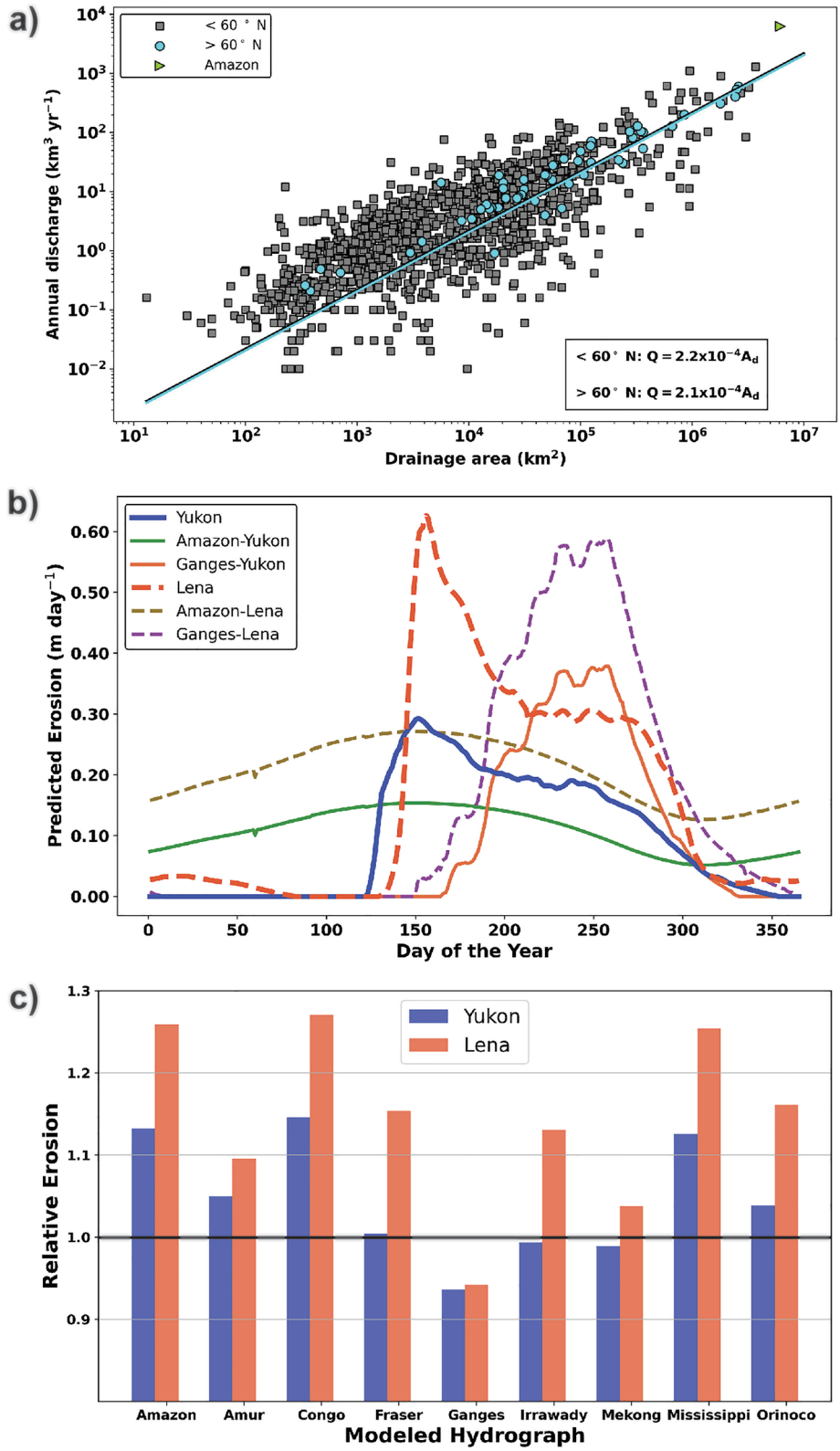

Figure 8.

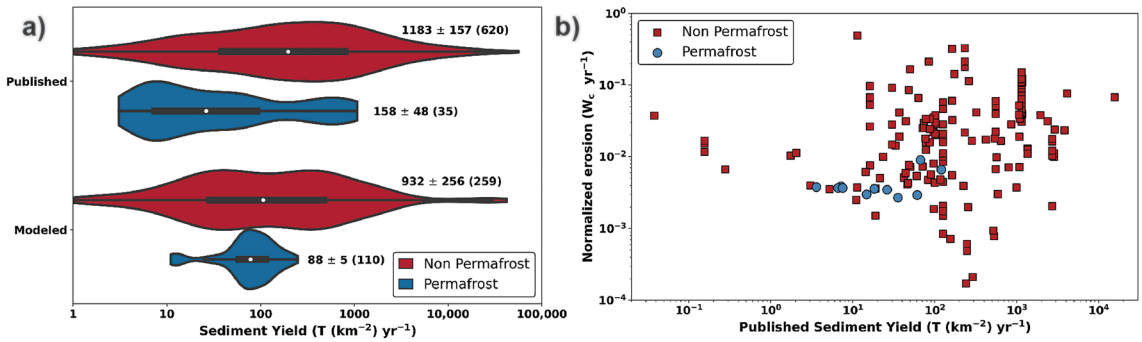

Figure 9. Comparison of permafrost and non-permafrost sediment yields and associated erosion rates. (a) Violin plots of published and modeled long-term average sediment yields (Cohen et al., 2013). The published data represent a combination of values reported in the L2S data set (Peucker-Ehrenbrink, 2009) and values published elsewhere in the literature (Rowland & Schwenk, 2019) https://data.ess-dive.lbl.gov/view/doi:10.15485/1571181. The rectangles display the interquartile range, the lines indicate the 1.5x interquartile range, white dots represent median values, and the displayed numbers are the mean, standard error, and number of observations (in parentheses). (b) Width-normalized erosion rates versus published sediment yield data.

provide more robust data sets of sediment flux to compare to permafrost riverbank erosion rates. However, based on the best currently available data, we conclude that it is unlikely that differences in sediment loads between permafrost and non-permafrost rivers provide a compelling alternative to permafrost as the dominant control on observed discrepancy in erosion rates.

5.4. A Stream Power Transition for Permafrost Influence on Riverbank Erosion Rates

The regression lines for erosion rates as a function of stream power permafrost and non-permafrost intersect at a stream power of 350 Wm^{-1}. This stream power value corresponds roughly to rivers less than 60 m wide or drainage areas ~1,000 km^2 (Figure S8 in Supporting Information S1). Given the uncertainty in the regression and variability in the data, we suggest that a change in scaling between permafrost and non-permafrost systems occurs over a transition between 350 and ~900 Wm^{-1} (drainage areas 1,000–10,000 km^2) and we hypothesize that the scaling relationship observed for our non-permafrost data set does not extend below values of 350 W m^{-1}. Below this transition, our observations suggest that erosion rates of rivers in permafrost settings may become largely transport limited such that bank retreat rates are limited by the occurrence of flows sufficient to mobilize already thawed sediments. Above this threshold, maximum bank erosion rates are limited by the rate at which frozen bank material may be thawed. The only two published studies of permafrost-affected rivers on systems with stream powers <350 W m^{-1} suggests that small Arctic rivers may have similar erosion dependence on stream power as we observed at lower latitudes.

In our permafrost data set, the Selawik River lies closest to this stream power transition. On this river we observe both transport and thaw-limited controls on bank erosion rates. At the rapidly eroding bank highlighted in Figure 7a and shown in Figure 1f, the river eroded less material than thaws seasonally in many years; a similar observation was made for the Usuktuk River in northern Alaska (Matsubara et al., 2015). Additionally, there exists a supply of readily transportable gravels throughout most of the summer, but few summer flows appear to be able to mobilize these sediments. In years of significant snowmelt-driven spring flooding, such as 2011, high transport rates appear to fully exhaust the supply of unfrozen bank materials and the thaw rate sets the upper limit of bank retreat (Figure 7b). On the Selawik River, the timing and rate of erosion also appear to be locally influenced by the bank grain size distributions and the presence and preservation of vegetated failure blocks. River ice may play a key role in removing these detached failure blocks and allowing renewed erosion of the banks.

Figure 8. Comparisons of permafrost and non-permafrost river basin hydrology. (a) Data from Land2Sea (Peucker-Ehrenbrink, 2009) separated into high (n = 54) and low (n = 1203) latitude river systems and plotted with annual discharge (Q) versus drainage area (A_d). Linear regression lines for both permafrost (blue) and non-permafrost (black) are plotted, but the black line is obscured by the blue line. The r^2 of the regressions are 0.96 for permafrost and 0.55 for non-permafrost rivers (p-values < 0.001). (b) Modeled daily erosion using Equation 2 for both the Yukon and Lena Rivers. The plot shows erosion based on observed long-term averaged daily flow for each river and for the same annual volume of flow temporally redistributed for two large non-permafrost rivers with high bank erosion rates and stream powers. (c) Predicted erosion for the Yukon and Lena Rivers using observed total annual discharge temporally distributed based on the average annual hydrographs of nine non-permafrost rivers. Values greater than one indicate that modeled erosion would be greater if the annual flow for the Yukon or Lena Rivers were redistributed in time equivalent to the non-permafrost river's flow regime.

Both the grain size of riverbanks and peak flow characteristics correlate to river basin size in ways that are consistent with smaller rivers being more transport-limited and larger rivers having a greater thermal control on erosion rates. Generally, bank materials become finer with larger upstream drainage basin areas (Knighton, 2014) and therefore a broader range of flows may be capable of transporting loose sediment away from thawing banks, thus reducing erosion dependence on transport conditions and increasing the relative importance of thermal controls. Ice content also tends to be higher in finer grained sediments (French & Shur, 2010). In many settings, increasing ice content slows bank erosion rates (Figure 6c) (Randriamazaoro et al., 2007; Shur et al., 2002; Williams, 1952), rendering riverbanks more thermally limited. Smaller rivers in the Arctic tend to have flashier hydrographs as measured by the ratio of maximum to mean annual discharges (Figure S12 in Supporting Information S1). Coarser, flashier, small rivers and streams likely erode under transport-limited threshold conditions set by bankfull or peak flows (Naito & Parker, 2019, 2020).

5.5. Scale-Dependent Response of Riverbank Erosion to Changing Climate in the Arctic

Our multitemporal analysis of erosion rates was limited to a few rivers and time periods, limiting our ability to assess changes in riverbank erosion rates due to historical climate forcings. We performed multitemporal analyses on the Yukon, Koyukuk, Noatak, and Lena Rivers but observed no clear pattern of temporal trends of rates greater than the observed interannual variability. On the Koyukuk River, however, analysis of high-resolution imagery provided differences in erosion rates greater than our levels of detection. Even though climate data for this region indicate that a 1°C increase in mean annual air temperature occurred between the time periods of our erosion analysis (1978–2012 and 2012–2018) (Harris et al., 2020), the temporal trends in rates were inconclusive; higher erosion rates occurred during the most recent time interval (2012–2018) at some but not all the sections and bends examined (Figure 6).

Potential climate drivers for changes in riverbank erosion rates in regions of permafrost include temperature, hydrology, sediment loads, and changes in river ice. In recent decades, the Arctic has warmed three times faster than the rest of the planet (AMAP, 2021) and is projected to continue to warm (Cai et al., 2021). Strong correlations between air and river temperatures (Yang & Peterson, 2017) portend increases in river temperatures and subsequent acceleration of riverbank erosion rates for rivers that are presently thaw limited (>900 Wm^{-1}, Figure 4b).

Though we do not find that hydrology explains regionally low rates of riverbank erosion, hydrology strongly influences rates and timing of erosion along individual permafrost rivers. Therefore, changes in hydrology in the Arctic may alter riverbank erosion rates. Projections suggest that hydrologically, northern rivers will shift from a nival (snowmelt) to more pluvial (rainfall) regime (Woo, 1990) with an increase in late summer flows (Lafrenière & Lamoureux, 2019) and extreme events (Nilsson et al., 2015). On larger rivers, a shift from snow melt dominated flow regimes to higher summer flows will combine with increased river temperatures to accelerate thermal erosion of banks (Dupeyrat et al., 2011). Floods may remove thawed bank materials more effectively and expose frozen banks to greater thermal erosion. A flattening of peak flows and more even distribution of discharge over the summer may also increase erosion on the largest Arctic rivers (Section 5.2, Figure 8c). On smaller rivers, a decrease in peak flows below critical thresholds for erosion may reduce bank erosion unless offset by larger magnitude summer floods.

The greening of the Arctic has been well documented (Myers-Smith et al., 2020) and is particularly pronounced in riparian settings (Naito & Cairns, 2011). On major rivers, vegetation colonization has been observed on newly accreted sedimentary deposits and bars (Brown et al., 2020; Ielpi et al., 2023). This vegetation expansion may stabilize islands and narrow channels (Ielpi et al., 2023), which in turn may alter river morphologies and erosion rates. To date, however, on rivers as large as those studied here, there is no clear documentation of increased vegetation colonization on actively eroding banks (Brown et al., 2020) and spring ice break up still appears highly effective at removing vegetated failure blocks.

Finally, a future reduction in winter ice cover (Chassiot et al., 2020) may reduce erosion rates across rivers of all sizes. On large rivers, abrasion and scour from local ice-jam flooding should decrease (Lininger & Wohl, 2019). On small rivers, less ice may leave protective vegetated failure blocks intact through the peak snowmelt floods and reduce bank erosion. For example, on the Selawik River, we observed 10 times greater erosion rates on bends where blocks were removed versus bends where blocks remained in place during major spring flows (Figure 7a).

6. Conclusions

For over 40 years, researchers have been unable to conclusively determine whether permafrost influences the rate of riverbank erosion relative to rivers without permafrost. Based on the pan-Arctic analysis, global meta-analysis of riverbank erosion, and field observations, we found a statistically significant nine times lower mean width-normalized erosion rate along riverbanks with permafrost compared to riverbanks lacking permafrost. At stream powers of <350–900 W m^{-1} (upstream drainage areas 1,000 to 10,000 km^2), we observed no difference between permafrost and non-permafrost rivers. Above this transition in stream power, however, the differences in erosion rates increase to a factor of 40 for the largest rivers in our data sets.

We conclude that permafrost is the most likely control on the relatively low bank erosion rates of permafrost rivers based on direct evidence from the Koyukuk, Selawik, and Yukon Rivers and a rejection of potential alternative hypotheses. Data from the Koyukuk River showed a reach and bend scale reduction in erosion rates as the fraction of permafrost in the surrounding floodplain increased. A lack of high-resolution and reliable permafrost maps at the pan-Arctic scale precluded a similar analysis along and between other rivers.

In both our pan-Arctic data set and detailed observations along individual rivers, erosion rates vary greatly even between banks with equivalent permafrost extent, however, the presence of permafrost does appear to set an upper limit on the maximum erosion rates. We suggest that this maximum limit is set by the rate at which frozen bank material may thaw and provide loose sediment for transport. Thermal sensors installed in a bend along the Selawik River, AK, appear to confirm this thaw limitation. Our data further suggest that this thaw limitation on bank erosion transitions to a transport limitation for rivers with stream powers below 350–900 W m^{-1}.

This apparent transition from thaw- to transport-limited erosion may exert a significant control on how rivers will respond to climate change in the Arctic. The erosion rates of thermally limited riverbanks of large rivers will likely increase as river temperatures increase and flow shifts from snowmelt dominated to higher discharges during the warmer summer months. Conversely, smaller transport-limited rivers may experience a decrease in erosion rates with a reduction in peak snow melt flows, unless these peak flows become offset by high-magnitude rain-driven floods. A decrease in river ice will likely also reduce erosion rates on both large and small rivers, but it is unlikely that at the watershed to pan-Arctic scale such reduction will offset the anticipated increases in thermally driven erosion rates for large rivers. Riverbank erosion represents a significant direct hazard to communities and infrastructure and associated changes in sediment and nutrient loading will likely impact fisheries and water quality. Our ability to predict and mitigate such impacts, however, will require additional data with higher spatial and temporal resolutions to better constrain permafrost extent and the mechanics, drivers, and timing of riverbank erosion in permafrost-affected floodplains.

Acknowledgments
Primary funding for this research was provided by the U.S. Department of Energy Office of Science Biological and Environmental Research Earth and Environmental Systems Sciences Division Early Career Award to J. Rowland, and the Regional and Global Model Analysis Program funded Interdisciplinary Research for Arctic Coastal Environments (InteRFACE) project awarded under contract Grant 89233218CNA000001 to Triad National Security, LLC ("Triad"). Additional funding was provided by Los Alamos National Laboratory Directed Research and Development for the work on Selawik River. Other funding sources for co-authors were provided by Caltech Terrestrial Hazards Observation and Reporting Center, Foster and Coco Stanback, the Linde Family, and the Resnick Sustainability Institute to Michael P. Lamb; National Science Foundation Awards 2127442 and 2031532; the National Defence Science and Engineering Graduate Fellowship for Madison M. Douglas and Preston C. Kemeny; and the Fannie and John Hertz Foundation Cohen/Jacobs and Stein Family Fellowship for Preston C. Kemeny. We thank the U.S. Fish and Wildlife Service Selawik National Wildlife Refuge for logistical support. Dana Brown, Mitchell Donovan, and Marc Van De Wiel provided data that supported the compilation of erosion rates. Logistical support was provided by Shawn Huffman, Alvin Attla, and Virgil Umphenour for work on the Koyukuk River. We thank Sheila Dufford, Clifford Adams, and the U.S. Fish and Wildlife Service for logistical support on the Yukon River. We thank the Koyukuk-hotana Athabascans, First Chief Norman Burgett, and the Huslia Tribal Council for land access and the USFWS–Koyukuk National Wildlife refuge for research permitting and logistical assistance. We thank Editor Amy East, reviewer Dongfeng Li, and an anonymous Associate Editor and reviewer for the time invested in providing constructive and valuable reviews of this manuscript.

Data Availability Statement

All original data and software used in this manuscript have been archived at the DOE ESS-DIVE data portal (http://ess-dive.lbl.gov/) and are cited and referenced in the manuscript. Data sets include global compilation of published erosion, https://data.ess-dive.lbl.gov/view/doi:10.15485/1571181 (Rowland & Schwenk, 2019); binary channel masks of Arctic rivers analyzed, https://data.ess-dive.lbl.gov/datasets/doi:10.15485/1571525 (Rowland & Stauffer, 2019a), erosion, accretion, and planform metrics of arctic rivers, https://data.ess-dive.lbl.gov/datasets/doi:10.15485/1571527 (Rowland & Stauffer, 2019b); bank temperature measurements measured on Selawik and Koyukuk Rivers, https://data.ess-dive.lbl.gov/datasets/doi:10.15485/1922885, (Rowland et al., 2023); and observations and map of permafrost along the Koyukuk River, https://data.ess-dive.lbl.gov/datasets/doi:10.15485/1922517, (Schwenk et al., 2023). The rabpro software can be accessed at https://doi.org/10.21105/joss.04237, (Schwenk et al., 2022).

References

Aalto, R., Lauer, J. W., & Dietrich, W. E. (2008). Spatial and temporal dynamics of sediment accumulation and exchange along Strickland River floodplains (Papua New Guinea) over decadal-to-centennial timescales. *Journal of Geophysical Research*, *113*(F1), F01S04. https://doi.org/10.1029/2006jf000627

Akhtar, M. P., Sharma, N. A. Y. A. N., & Ojha, C. S. P. (2011). Braiding process and bank erosion in the Brahmaputra River. *International Journal of Sediment Research*, *26*(4), 431–444. https://doi.org/10.1016/S1001-6279(12)60003-1

AMAP. (2021). Arctic climate change update 2021: Key trends and impacts. Summary for policy-makers. In *Tromsø, Norway: Arctic monitoring and assessment programme (AMAP)* (pp. 1–16).

Are, F. E. (1983). Thermal abrasion of coasts. In *Presented at the proceedings of the fourth international conference on permafrost* (pp. 24–28).
Barbarossa, V., Huijbregts, M. A. J., Beusen, A. H. W., Beck, H. E., King, H., & Schipper, A. M. (2018). Data descriptor: FLO1K, global maps of mean, maximum and minimum annual streamflow at 1 km resolution from 1960 through 2015. *Scientific Data*, *5*, 180052. https://doi.org/10.1038/sdata.2018.52
Barnhart, T. B., & Crosby, B. T. (2013). Comparing two methods of surface change detection on an evolving thermokarst using high-temporal-frequency terrestrial laser scanning, Selawik River, Alaska. *Remote Sensing*, *5*(6), 2813–2837. https://doi.org/10.3390/rs5062813
Beck, H. E., Zimmermann, N. E., McVicar, T. R., Vergopolan, N., Berg, A., & Wood, E. F. (2018). Present and future Köppen-Geiger climate classification maps at 1-km resolution. *Scientific Data*, *5*, 1–12. https://doi.org/10.1038/sdata.2018.214
Best, H., McNamara, J. P., & Liberty, L. (2005). Association of ice and river channel morphology determined using ground-penetrating radar in the Kuparuk River, Alaska. *Arctic Antarctic and Alpine Research*, *37*(2), 157–162. https://doi.org/10.1657/1523-0430(2005)037[0157:AOIARC]2.0.CO;2
Bizzi, S., & Lerner, D. N. (2015). The use of stream power as an indicator of channel sensitivity to erosion and deposition processes. *River Research and Applications*, *31*(1), 16–27. https://doi.org/10.1002/rra.2717
Blume-Werry, G., Milbau, A., Teuber, L. M., Johansson, M., & Dorrepaal, E. (2019). Dwelling in the deep—Strongly increased root growth and rooting depth enhance plant interactions with thawing permafrost soil. *New Phytologist*, *223*(3), 1328–1339. https://doi.org/10.1111/nph.15903
Boucher, É., Bégin, Y., & Arseneault, D. (2009). Impacts of recurring ice jams on channel geometry and geomorphology in a small high-boreal watershed. *Geomorphology*, *108*(3–4), 273–281. https://doi.org/10.1016/j.geomorph.2009.02.014
Brinkman, T. J., Hansen, W. D., Iii, F. S. C., Kofinas, G., Burnsilver, S., & Rupp, T. S. (2016). Arctic communities perceive climate impacts on access as a critical challenge to availability of subsistence resources. *Climatic Change*, *139*(3–4), 413–427. https://doi.org/10.1007/s10584-016-1819-6
Brown, D. R. N., Brinkman, T. J., Bolton, W. R., Brown, C. L., Cold, H. S., Hollingsworth, T. N., & Verbyla, D. L. (2020). Implications of climate variability and changing seasonal hydrology for subarctic riverbank erosion. *Climatic Change*, *162*(2), 385–404. https://doi.org/10.1007/s10584-020-02748-9
Brown, J. O., Heginbottom, J. A., & Melnikov, E. (2002). *Circum-Arctic map of permafrost and ground-ice conditions, version 2*. NSIDC: National Snow and Ice Data Center. https://doi.org/10.7265/skbg-kf16
Bufe, A., Paola, C., & Burbank, D. W. (2016). Fluvial bevelling of topography controlled by lateral channel mobility and uplift rate. *Nature Geoscience*, *9*(9), 706–710. https://doi.org/10.1038/ngeo2773
Cable, W. L., Romanovsky, V. E., & Jorgenson, M. T. (2016). Scaling-up permafrost thermal measurements in western Alaska using an ecotype approach. *The Cryosphere*, *10*(5), 2517–2532. https://doi.org/10.5194/tc-10-2517-2016
Cai, Z., You, Q., Wu, F., Chen, H. W., Chen, D., & Cohen, J. (2021). Arctic warming revealed by multiple CMIP6 models: Evaluation of historical simulations and quantification of future projection uncertainties. *Journal of Climate*, *34*(12), 4871–4892. https://doi.org/10.1175/JCLI-D-20-0791.1
Chassiot, L., Lajeunesse, P., & Bernier, J. F. (2020). Riverbank erosion in cold environments: Review and outlook. *Earth-Science Reviews*, *207*, 103231. https://doi.org/10.1016/j.earscirev.2020.103231
Church, M. (1977). River studies in northern Canada: Reading the record from river morphology. *Geoscience Canada*, *4*(1).
Clement, D. T. (1999). *Fluvial geomorphology of the Yukon River, Yukon Flats*. University of Calgary.
Cohen, S., Kettner, A. J., Syvitski, J. P. M., & Fekete, B. M. (2013). WBMsed, a distributed global-scale riverine sediment flux model: Model description and validation. *Computers & Geosciences*, *53*, 80–93. https://doi.org/10.1016/j.cageo.2011.08.011
Cold, H. S., Brinkman, T. J., Brown, C. L., Hollingsworth, T. N., Brown, D. R. N., & Heeringa, K. M. (2020). Assessing vulnerability of subsistence travel to effects of environmental change in Interior Alaska. *Ecology and Society*, *25*(1), art20. https://doi.org/10.5751/es-11426-250120
Constantine, J. A., Dunne, T., Ahmed, J., Legleiter, C., & Lazarus, E. D. (2014). Sediment supply as a driver of river meandering and floodplain evolution in the Amazon Basin. *Nature Geoscience*, *7*(12), 899–903. https://doi.org/10.1038/ngeo2282
Cooper, R. H., & Hollingshead, A. B. (1973). River bank erosion in regions of permafrost. In *Proceedings of the hydrology symposium. Subcommittee on hydrology by the inland waters directorate* (Vol. 9, pp. 272–283). Department of the Environment.
Costard, F., Dupeyrat, L., Gautier, E., & Carey-Gailhardis, E. (2003). Fluvial thermal erosion investigations along a rapidly eroding river bank: Application to the Lena River (central Siberia). *Earth Surface Processes and Landforms*, *28*(12), 1349–1359. https://doi.org/10.1002/esp.592
Costard, F., & Gautier, E. (2007). The Lena River: Hydromorphodynamic features in a deep permafrost zone. *Large Rivers: Geomorphology and Management*, 225–233.
Costard, F., Gautier, E., Fedorov, A., Konstantinov, P., & Dupeyrat, L. (2014). An assessment of the erosion potential of the fluvial thermal process during ice breakups of the Lena River (Siberia). *Permafrost and Periglacial Processes*, *25*(3), 162–171. https://doi.org/10.1002/ppp.1812
Dai, A., & Trenberth, K. E. (2002). Estimates of freshwater discharge from continents: Latitudinal and seasonal variations. *Journal of Hydrometeorology*, *3*(6), 660–687. https://doi.org/10.1175/1525-7541(2002)003<0660:eofdfc>2.0.co;2
Darby, S. E., Rinaldi, M., & Dapporto, S. (2007). Coupled simulations of fluvial erosion and mass wasting for cohesive river banks. *Journal of Geophysical Research*, *112*(F3), F03022. https://doi.org/10.1029/2006jf000722
Darby, S. E., & Thorne, C. R. (1996). Development and testing of riverbank-stability analysis by Stephen E. Darby 1 and Colin R. Thorne, 2 affiliate member, ASCE. *Journal of Hydraulic Engineering*, *122*, 443–454. https://doi.org/10.1061/(asce)0733-9429(1996)122:8(443)
Darby, S. E., Trieu, H. Q., Carling, P. A., Sarkkula, J., Koponen, J., Kummu, M., et al. (2010). A physically based model to predict hydraulic erosion of fine-grained riverbanks: The role of form roughness in limiting erosion. *Journal of Geophysical Research*, *115*(F4), 115. https://doi.org/10.1029/2010jf001708
Debol'skaya, E. I., & Ivanov, A. V. (2020). Comparative analysis of models of thermoerosion-induced channel deformations in rivers of permafrost zone. *Water Resources*, *47*(1), 77–86. https://doi.org/10.1134/S0097807820010054
Dietrich, E. (1999). The Fly River, Papua New Guinea: Inferences about river dynamics, floodplain sedimentation and fate of sediment. In A. J. Miller, & A. Gupta (Eds.), *Varieties of fluvial forms*. John Wiley & Sons, Ltd.
Dingle, E. H., Sinclair, H. D., Venditti, J. G., Attal, M., Kinnaird, T. C., Creed, M., et al. (2020). Sediment dynamics across gravel-sand transitions: Implications for river stability and floodplain recycling. *Geology*, *48*(5), 468–472. https://doi.org/10.1130/G46909.1
Donovan, M., & Belmont, P. (2019). Timescale dependence in river channel migration measurements. *Earth Surface Processes and Landforms*, *44*(8), 1530–1541. https://doi.org/10.1002/esp.4590
Donovan, M., Belmont, P., Notebaert, B., Coombs, T., Larson, P., & Souffront, M. (2019). Accounting for uncertainty in remotely-sensed measurements of river planform change. *Earth-Science Reviews*, *193*, 220–236. https://doi.org/10.1016/j.earscirev.2019.04.009

Donovan, M., Belmont, P., & Sylvester, Z. (2021). Evaluating the relationship between meander-bend curvature, sediment supply, and migration rates. *Journal of Geophysical Research: Earth Surface*, *126*(3), 1–20. https://doi.org/10.1029/2020JF006058

Douglas, M. M., Dunne, K. B. J., & Lamb, M. P. (2023). Sediment entrainment and slump blocks limit permafrost riverbank erosion. *Geophyscial Research Letters*, *50*(11), e2023GL102974. https://doi.org/10.1029/2023gl102974

Douglas, M. M., Li, G. K., Fischer, W. W., Rowland, J. C., Kemeny, P. C., West, A. J., et al. (2022). Organic carbon burial by river meandering partially offsets bank erosion carbon fluxes in a discontinuous permafrost floodplain. *Earth Surface Dynamics*, *10*(3), 421–435. https://doi.org/10.5194/esurf-10-421-2022

Drake, T. W., Guillemette, F., Hemingway, J. D., Chanton, J. P., Podgorski, D. C., Zimov, N. S., & Spencer, R. G. M. (2018). The ephemeral signature of permafrost carbon in an Arctic fluvial network. *Journal of Geophysical Research: Biogeosciences*, *123*(5), 1475–1485. https://doi.org/10.1029/2017JG004311

Dunne, T., Constantine, J. A., & Singer, M. (2010). The role of sediment transport and sediment supply in the evolution of river channel and floodplain complexity. *Transactions—Japanese Geomorphological Union*, *31*(2), 155–170.

Dunne, T., Dietrich, W. E., Humphrey, N. F., & Tubbs, D. W. (1981). Geologic and geomorphic implications for gravel supply. In *Presented at the proceedings of the conference on Salmon-spawning gravel: A renewable resource in the Pacific northwest* (pp. 75–100).

Dupeyrat, L., Costard, F., Randriamazaoro, R., Gailhardis, E., Gautier, E., & Fedorov, A. (2011). Effects of ice content on the thermal erosion of permafrost: Implications for coastal and fluvial erosion. *Permafrost and Periglacial Processes*, *22*(2), 179–187. https://doi.org/10.1002/ppp.722

Eardley, A. J. (1938). Yukon channel shifting. *Bulletin of the Geological Society of America*, *49*(3), 343–358. https://doi.org/10.1130/gsab-49-343

Ettema, R. (2002). Review of alluvial-channel responses to river ice. *Journal of Cold Regions Engineering*, *16*(4), 191–217. https://doi.org/10.1061/(ASCE)0887-381X(2002)16:4(191)

Flanders, D., Hall-Beyer, M., & Pereverzoff, J. (2003). Preliminary evaluation of eCognition object-based software for cut block delineation and feature extraction. *Canadian Journal of Remote Sensing*, *29*(4), 441–452. https://doi.org/10.5589/m03-006

Francalanci, S., Lanzoni, S., Solari, L., & Papanicolaou, A. N. (2020). Equilibrium cross section of river channels with cohesive erodible banks. *Journal of Geophysical Research: Earth Surface*, *125*(1), 1–20. https://doi.org/10.1029/2019JF005286

French, H. (2007). *The periglacial environment* (Vol. 3). John Wiley & Sons, Ltd. Retrieved from http://alamos.eblib.com/patron/FullRecord.aspx?p=291041

French, H., & Shur, Y. (2010). The principles of cryostratigraphy. *Earth-Science Reviews*, *101*(3–4), 190–206. https://doi.org/10.1016/j.earscirev.2010.04.002

Gatto, L. W. (1984). Bank and channel changes near Dikes, Tanana River, Alaska. In C. M. Elliott (Ed.), *River meandering, proceedings of the conference Rivers '83* (pp. 212–222).

Gautier, E., Dépret, T., Cavero, J., Costard, F., Virmoux, C., Fedorov, A., et al. (2021). Fifty-year dynamics of the Lena River islands (Russia): Spatio-temporal pattern of large periglacial anabranching river and influence of climate change. *Science of the Total Environment*, *783*, 147020. https://doi.org/10.1016/j.scitotenv.2021.147020

Gordeev, V. V. (2006). Fluvial sediment flux to the Arctic Ocean. *Geomorphology*, *80*(1–2), 94–104. https://doi.org/10.1016/j.geomorph.2005.09.008

Gruber, S. (2012). Derivation and analysis of a high-resolution estimate of global permafrost zonation. *The Cryosphere*, *6*(1), 221–233. https://doi.org/10.5194/tc-6-221-2012

Gustafsson, O., van Dongen, B. E., Vonk, J. E., Dudarev, O. V., & Semiletov, I. P. (2011). Widespread release of old carbon across the Siberian Arctic echoed by its large rivers. *Biogeosciences*, *8*(6), 1737–1743. https://doi.org/10.5194/bg-8-1737-2011

Harris, I., Osborn, T. J., Jones, P., & Lister, D. (2020). Version 4 of the CRU TS monthly high-resolution gridded multivariate climate dataset. *Scientific Data*, *7*(1), 109. https://doi.org/10.1038/s41597-020-0453-3

Hickin, E. J., & Nanson, G. C. (1984). Lateral migration rates of river bends. *Journal of Hydraulic Engineering*, *110*(11), 1557–1567. https://doi.org/10.1061/(asce)0733-9429(1984)110:11(1557)

Hinzman, L. D., Kane, D. L., & Woo, M. (2005). Permafrost hydrology. In M. Anderson (Ed.), *Encyclopedia of hydrological sciences* (Vol. 4, pp. 2679–2693). John Wiley.

Holmes, R. M., Coe, M. T., Fiske, G. J., Gurtovaya, T., Mcclelland, J. W., Shiklomanov, A. I., et al. (2012). Climate change impacts on the hydrology and biogeochemistry of Arctic rivers. In C. R. Goldman, M. Kumagai, & R. D. Robarts (Eds.), *Climatic change and global warming of inland waters: Impacts and mitigation for ecosystems and societies* (pp. 1–26). John Wiley & Sons, Ltd. https://doi.org/10.1002/9781118470596.ch1

Holmes, R. M., McClelland, J. W., Peterson, B. J., Tank, S. E., Bulygina, E., Eglinton, T. I., et al. (2012). Seasonal and annual fluxes of nutrients and organic matter from large rivers to the Arctic Ocean and surrounding seas. *Estuaries and Coasts*, *35*(2), 369–382. https://doi.org/10.1007/s12237-011-9386-6

Holmgren, W. F., Hansen, C. W., & Mikofski, M. A. (2018). pvlib python: A python package for modeling solar energy systems. *Journal of Open Source Software*, *3*(29), 884. https://doi.org/10.21105/JOSS.00884

Hooke, J. M. (1980). Magnitude and distribution of rates of river bank erosion. *Earth Surface Processes*, *5*(2), 143–157. https://doi.org/10.1002/esp.3760050205

Hovelsrud, G. K., Poppel, B., Van Oort, B., & Reist, J. D. (2011). Arctic societies, cultures, and peoples in a changing cryosphere. *Ambio*, *40*(1), 100–110. https://doi.org/10.1007/s13280-011-0219-4

Ielpi, A., & Lapôtre, M. G. A. (2020). A tenfold slowdown in river meander migration driven by plant life. *Nature Geoscience*, *13*(1), 82–86. https://doi.org/10.1038/s41561-019-0491-7

Ielpi, A., Lapôtre, M. G. A., Finotello, A., & Roy-Léveillée, P. (2023). Large sinuous rivers are slowing down in a warming Arctic. *Nature Climate Change*, *13*(4), 375–381. https://doi.org/10.1038/s41558-023-01620-9

Instanes, A., Kokorev, V., Janowicz, R., Bruland, O., Sand, K., & Prowse, T. (2016). Changes to freshwater systems affecting Arctic infrastructure and natural resources. *Journal of Geophysical Research: Biogeosciences*, *121*(3), 567–585. https://doi.org/10.1002/2015jg003125

Jackson, R. B., Canadell, J., Ehleringer, J. R., Mooney, H. A., Sala, O. E., & Schulze, E. D. (1996). A global analysis of root distributions for terrestrial biomes. *Oecologia*, *108*(3), 389–411. https://doi.org/10.1007/BF00333714

Jorgenson, M. T., Roth, J. E., Miller, F. P., Macander, M. J., Duffy, M. S., Wells, A. F., et al. (2009). *An ecological land survey and landcover map of the Selawik national wildlife refuge* (pp. 1–307). Natural Resource Technical Report.

Kanevskiy, M., Shur, Y., Strauss, J., Jorgenson, T., Fortier, D., Stephani, E., & Vasiliev, A. (2016). Patterns and rates of riverbank erosion involving ice-rich permafrost (yedoma) in northern Alaska. *Geomorphology*, *253*, 370–384. https://doi.org/10.1016/j.geomorph.2015.10.023

Knighton, D. (2014). *Fluvial forms and processes: A new perspective*. Routledge.

Krasnoshchekov, S. Y. (2009). *Determining lateral river channel activity with respect to safety of pipeline crossings*. University of Southampton.

Lafrenière, M. J., & Lamoureux, S. F. (2019). Effects of changing permafrost conditions on hydrological processes and fluvial fluxes. *Earth-Science Reviews*, *191*, 212–223. https://doi.org/10.1016/j.earscirev.2019.02.018

Langhorst, T., & Pavelsky, T. (2023). Global observations of riverbank erosion and accretion from Landsat imagery. *Journal of Geophysical Research: Earth Surface*, *128*(2), e2022JF006774. https://doi.org/10.1029/2022JF006774

Larsen, E. W., Premier, A. K., & Greco, S. E. (2006). Cumulative effective stream power and bank erosion on the Sacramento River, California, USA. *Journal of the American Water Resources Association*, *42*(4), 1077–1097. https://doi.org/10.1111/j.1752-1688.2006.tb04515.x

Lawler, D. M., Grove, J. R., Couperthwaite, J. S., & Leeks, G. J. L. (1999). Downstream change in river bank erosion rates in the Swale–Ouse system, northern England. *Hydrological Processes*, *13*(7), 977–992. https://doi.org/10.1002/(sici)1099-1085(199905)13:7<977::aid-hyp785>3.0.co;2-5

Lawson, D. E. (1983). *CRREL report 83-29 Erosion of perennially frozen streambanks* (p. 22). Hanover, N.H.: U.S. Army Corps of Engineers, Cold Regions Research and Engineering Laboratory.

Leffingwell, E. K. (1919). *The Canning River region, northern Alaska. USGS professional paper 109* (p. 251). Government Printing Office.

Leyland, J., Darby, S. E., Teruggi, L., Rinaldi, M., & Ostuni, D. (2015). A self-limiting bank erosion mechanism? Inferring temporal variations in bank form and skin drag from high resolution topographic data. *Earth Surface Processes and Landforms*, *40*(12), 1600–1615. https://doi.org/10.1002/esp.3739

Lin, P., Pan, M., Allen, G. H., de Frasson, R. P., Zeng, Z., Yamazaki, D., & Wood, E. F. (2020). Global estimates of reach-level Bankfull River width leveraging big data geospatial analysis. *Geophysical Research Letters*, *47*(7), 1–12. https://doi.org/10.1029/2019GL086405

Lininger, K. B., & Wohl, E. (2019). Earth-science reviews floodplain dynamics in North American permafrost regions under a warming climate and implications for organic carbon stocks: A review and synthesis. *Earth-Science Reviews*, *193*, 24–44. https://doi.org/10.1016/j.earscirev.2019.02.024

Lininger, K. B., Wohl, E., & Rose, J. R. (2018). Geomorphic controls on floodplain soil organic carbon in the Yukon Flats, interior Alaska, from reach to river basin scales. *Water Resources Research*, *54*(3), 1934–1951. https://doi.org/10.1002/2017wr022042

Lininger, K. B., Wohl, E., Rose, J. R., & Leisz, S. J. (2019). Significant floodplain soil organic carbon storage along a large high-latitude river and its tributaries. *Geophysical Research Letters*, *46*(4), 2121–2129. https://doi.org/10.1029/2018gl080996

Mann, P. J., Eglinton, T. I., Mcintyre, C. P., Zimov, N., Davydova, A., Vonk, J. E., et al. (2015). Utilization of ancient permafrost carbon in headwaters of Arctic fluvial networks. *Nature Communications*, *6*, 1–7. https://doi.org/10.1038/ncomms8856

Matsubara, Y., Howard, A. D., Burr, D. M., Williams, R. M. E., Dietrich, W. E., & Moore, J. M. (2015). River meandering on Earth and Mars: A comparative study of Aeolis Dorsa meanders, Mars and possible terrestrial analogs of the Usuktuk River, AK, and the Quinn River, NV. *Geomorphology*, *240*, 102–120. https://doi.org/10.1016/j.geomorph.2014.08.031

McClelland, J. W., Holmes, R. M., Peterson, B. J., Raymond, P. A., Striegl, R. G., Zhulidov, A. V., et al. (2016). Particulate organic carbon and nitrogen export from major Arctic rivers. *Global Biogeochemical Cycles*, *30*(5), 629–643. https://doi.org/10.1002/2015gb005351

McNamara, J. P., & Kane, D. L. (2009). The impact of a shrinking cryosphere on the form of arctic alluvial channels. *Hydrological Processes*, *23*(1), 159–168. https://doi.org/10.1002/HYP.7199

Midgley, T. L., Fox, G. A., & Heeren, D. M. (2012). Evaluation of the bank stability and toe erosion model (BSTEM) for predicting lateral retreat on composite streambanks. *Geomorphology*, *145*, 107–114. https://doi.org/10.1016/j.geomorph.2011.12.044

Miles, M. (1976). *An investigation on riverbanks and coastal erosion, Banks Island, District of Franklin* (pp. 195–200). Geological Survey of Canada.

Milliman, J. D., & Farnsworth, K. L. (2013). *River discharge to the coastal ocean: A global synthesis*. Cambridge University Press.

Moody, J. A. (2022). The effects of discharge and bank orientation on the annual riverbank erosion along Powder River in Montana, USA. *Geomorphology*, *403*, 108134. https://doi.org/10.1016/J.GEOMORPH.2022.108134

Myers-Smith, I. H., Kerby, J. T., Phoenix, G. K., Bjerke, J. W., Epstein, H. E., Assmann, J. J., et al. (2020). Complexity revealed in the greening of the Arctic. *Nature Climate Change*, *10*(2), 106–117. https://doi.org/10.1038/s41558-019-0688-1

Naito, A. T., & Cairns, D. M. (2011). Relationships between Arctic shrub dynamics and topographically derived hydrologic characteristics. *Environmental Research Letters*, *6*(4), 045506. https://doi.org/10.1088/1748-9326/6/4/045506

Naito, K., & Parker, G. (2019). Can bankfull discharge and bankfull channel characteristics of an alluvial meandering river be cospecified from a flow duration curve? *Journal of Geophysical Research: Earth Surface*, *124*(10), 2381–2401. https://doi.org/10.1029/2018JF004971

Naito, K., & Parker, G. (2020). Adjustment of self-formed bankfull channel geometry of meandering rivers: Modelling study. *Earth Surface Processes and Landforms*, *45*(13), 3313–3322. https://doi.org/10.1002/esp.4966

Nanson, G. C., & Hickin, E. J. (1986). A statistical analysis of bank erosion and channel migration in western Canada. *Geological Society of America Bulletin*, *97*(4), 497–504. https://doi.org/10.1130/0016-7606(1986)97<497:asaobe>2.0.co;2

Nilsson, C., Polvi, L. E., & Lind, L. (2015). Extreme events in streams and rivers in arctic and subarctic regions in an uncertain future. *Freshwater Biology*, *60*(12), 2535–2546. https://doi.org/10.1111/fwb.12477

Obu, J., Westermann, S., Bartsch, A., Berdnikov, N., Christiansen, H. H., Dashtseren, A., et al. (2019). Northern Hemisphere permafrost map based on TTOP modelling for 2000–2016 at 1 km^2 scale. *Earth-Science Reviews*, *193*, 299–316. https://doi.org/10.1016/j.earscirev.2019.04.023

Obu, J., Westermann, S., Kääb, A., & Bartsch, A. (2018). *Ground temperature map, 2000-2016, northern hemisphere permafrost*. PANGAEA. https://doi.org/10.1594/PANGAEA.888600

Partheniades, E. (1965). Erosion and deposition of cohesive soils. *Journal of the Hydraulics Division*, *91*(1), 105–139. https://doi.org/10.1061/jyceaj.0001165

Pastick, N. J., Jorgenson, M. T., Wylie, B. K., Nield, S. J., Johnson, K. D., & Finley, A. O. (2015). Distribution of near-surface permafrost in Alaska: Estimates of present and future conditions. *Remote Sensing of Environment*, *168*, 301–315. https://doi.org/10.1016/j.rse.2015.07.019

Pastick, N. J., Jorgenson, M. T., Wylie, B. K., Rose, J. R., Rigge, M., & Walvoord, M. A. (2014). Spatial variability and landscape controls of near-surface permafrost within the Alaskan Yukon River Basin. *Journal of Geophysical Research: Biogeosciences*, *119*(6), 1244–1265. https://doi.org/10.1002/2013jg002594

Payne, C., Panda, S., & Prakash, A. (2018). Remote sensing of river erosion on the Colville River, North Slope Alaska. *Remote Sensing*, *10*(3), 397. https://doi.org/10.3390/rs10030397

Perkins, S. J., Edlund, K., Esch-Mosher, D., Eads, D., Harvey, N., & Brumby, S. (2005). Genie Pro: Robust image classification using shape, texture, and spectral information. *Proceedings of SPIE*, *5806*, 139–148.

Peucker-Ehrenbrink, B. (2009). Land2Sea database of river drainage basin sizes, annual water discharges, and suspended sediment fluxes. *Geochemistry, Geophysics, Geosystems*, *10*(6), Q06014. https://doi.org/10.1029/2008gc002356

Pizzuto, J. (2009). An empirical model of event scale cohesive bank profile evolution. *Earth Surface Processes and Landforms*, *34*, 1234–1244. https://doi.org/10.1002/esp

Prowse, T. D., & Beltaos, S. (2002). Climatic control of river-ice hydrology: A review. *Hydrological Processes*, *16*(4), 805–822. https://doi.org/10.1002/hyp.369

Prowse, T. D., & Culp, J. M. (2003). Ice breakup: A neglected factor in river ecology. *Canadian Journal of Civil Engineering*, *30*(1), 128–144. https://doi.org/10.1139/l02-040

Rachold, V., Eicken, H., Gordeev, V. V., Grigoriev, M. N., Hubberten, H. W., Lisitzin, A. P., et al. (2004). Modern terrigenous organic carbon input to the Arctic Ocean. In R. Stein, & R. W. Macdonald (Eds.), *The organic carbon cycle in the Arctic Ocean* (p. 378). Springer-Verlag. https://doi.org/10.1007/978-3-642-18912-8

Randriamazaoro, R., Dupeyrat, L., Costard, F., & Gailhardis, E. C. (2007). Fluvial thermal erosion: Heat balance integral method. *Earth Surface Processes and Landforms*, *32*(12), 1828–1840. https://doi.org/10.1002/esp.1489

Raynolds, M. K., Walker, D. A., Balser, A., Bay, C., Campbell, M., Cherosov, M. M., et al. (2019). A raster version of the Circumpolar Arctic Vegetation Map (CAVM). *Remote Sensing of Environment*, *232*, 111297. https://doi.org/10.1016/j.rse.2019.111297

Rinaldi, M., & Casagli, N. (1999). Stability of streambanks formed in partially saturated soils and effects of negative pore water pressures: The Sieve River (Italy). *Geomorphology*, *26*(4), 253–277. https://doi.org/10.1016/S0169-555X(98)00069-5

Rinaldi, M., & Darby, S. E. (2007). Modelling river-bank-erosion processes and mass failure mechanisms: Progress towards fully coupled simulations. In *Developments in Earth surface processes* (Vol. 11, pp. 213–239). Elsevier. https://doi.org/10.1016/S0928-2025(07)11126-3

Rinaldi, M., Mengoni, B., Luppi, L., Darby, S. E., & Mosselman, E. (2008). Numerical simulation of hydrodynamics and bank erosion in a river bend. *Water Resources Research*, *44*(9), 1–17. https://doi.org/10.1029/2008WR007008

Rowland, J. C., Crosby, B., Schwenk, J., Piliouras, A., & Douglas, M. (2023). Riverbank temperatures on the Selawik River, Alaska 2010-2012, and Koyukuk River, Alaska June to July 2018. Incorporating the hydrological controls on carbon cycling in floodplain ecosystems into Earth system models (ESMs), ESS-DIVE repository [Dataset]. ESS-DIVE. https://doi.org/10.15485/1922885

Rowland, J. C., & Schwenk, J. (2019). Global meta-analysis of published river bank erosion and migration rates [Dataset]. ESS-DIVE. https://doi.org/10.15485/1571181

Rowland, J. C., Shelef, E., Pope, P. A., Muss, J., Gangodagamage, C., Brumby, S. P., & Wilson, C. J. (2016). A morphology independent methodology for quantifying planview river change and characteristics from remotely sensed imagery. *Remote Sensing of Environment*, *184*, 212–228. https://doi.org/10.1016/j.rse.2016.07.005

Rowland, J. C., & Stauffer, S. (2019a). Classified channel masks of portions of 13 rivers across the Arctic and areas of floodplain erosion and accretion ranging from 1973 to 2016 [Dataset]. ESS-DIVE. https://doi.org/10.15485/1571525

Rowland, J. C., & Stauffer, S. (2019b). Pan-arctic river bank erosion and accretion, and planform metrics measured over intervals ranging from 1973 to 2016 [Dataset]. ESS-DIVE. https://doi.org/10.15485/1571527

Schuur, E. A. G., McGuire, A. D., Schädel, C., Grosse, G., Harden, J. W., Hayes, D. J., et al. (2015). Climate change and the permafrost carbon feedback. *Nature*, *520*(7546), 171–179. https://doi.org/10.1038/nature14338

Schwenk, J., Khandelwal, A., Fratkin, M., Kumar, V., & Foufoula-Georgiou, E. (2017). High spatiotemporal resolution of river planform dynamics from Landsat: The RivMAP toolbox and results from the Ucayali River. *Earth and Space Science*, *4*(2), 46–75. https://doi.org/10.1002/2016ea000196

Schwenk, J., Piliouras, A., & Rowland, J. C. (2023). Observations and machine-learned models of near-surface permafrost along the Koyukuk River, Alaska, USA. Incorporating the hydrological controls on carbon cycling in floodplain ecosystems into Earth system models (ESMs), ESS-DIVE repository [Dataset]. ESS-DIVE. https://doi.org/10.15485/1922517

Schwenk, J., Zussman, T., Stachelek, J., & Rowland, J. C. (2022). Rabpro: Global watershed boundaries, river elevation profiles, and catchment statistics [Software]. Journal of Open Source Software, *7*(73), 4237. https://doi.org/10.21105/joss.04237

Scott, K. M. (1978). *Effects of permafrost on stream channel behavior in Arctic Alaska*. US Government Printing Office.

Scrimgeour, G. J., Prowse, T. D., Culp, J. M., & Chambers, P. A. (1994). Ecological effects of river ice break-up: A review and perspective. *Freshwater Biology*, *32*(2), 261–275. https://doi.org/10.1111/j.1365-2427.1994.tb01125.x

Shur, Y., Jones, B. M., Kanevskiy, M., Jorgenson, T., Jones, M. K. W., Fortier, D., et al. (2021). Fluvio-thermal erosion and thermal denudation in the yedoma region of northern Alaska: Revisiting the Itkillik River exposure. *Permafrost and Periglacial Processes*, *32*(2), 277–298. https://doi.org/10.1002/ppp.2105

Shur, Y., Vasiliev, A., Kanevsky, M., Maximov, V., Pokrovsky, S., & Zaikanov, V. (2002). Shore erosion in Russian Arctic. In *Cold regions engineering cold regions impacts on transportation and infrastructure: Proceedings of the eleventh international conference* (pp. 736–747). https://doi.org/10.1061/40621(254)63

Simon, A., & Collison, A. J. C. (2002). Quantifying the mechanical and hydrologic effects of riparian vegetation on streambank stability. *Earth Surface Processes and Landforms*, *27*(5), 527–546. https://doi.org/10.1002/ESP.325

Stettner, S., Beamish, A. L., Bartsch, A., Heim, B., Grosse, G., Roth, A., & Lantuit, H. (2018). Monitoring inter- and intra-seasonal dynamics of rapidly degrading ice-rich permafrost riverbanks in the Lena Delta with TerraSAR-X time series. *Remote Sensing*, *10*(1), 51. https://doi.org/10.3390/rs10010051

Striegl, R. G., Dornblaser, M. M., Aiken, G. R., Wickland, K. P., & Raymond, P. A. (2007). Carbon export and cycling by the Yukon, Tanana, and Porcupine rivers, Alaska, 2001-2005. *Water Resources Research*, *43*(2), 2001–2005. https://doi.org/10.1029/2006WR005201

Tananaev, N. (2016). Hydrological and sedimentary controls over fluvial thermal erosion, the Lena River, central Yakutia. *Geomorphology*, *253*, 524–533. https://doi.org/10.1016/j.geomorph.2015.11.009

Tananaev, N., & Lotsari, E. (2022). Defrosting northern catchments: Fluvial effects of permafrost degradation. *Earth-Science Reviews*, *228*, 103996. https://doi.org/10.1016/j.earscirev.2022.103996

Tank, S. E., Raymond, P. A., Striegl, R. G., McClelland, J. W., Holmes, R. M., Fiske, G. J., & Peterson, B. J. (2012). A land-to-ocean perspective on the magnitude, source and implication of DIC flux from major Arctic rivers to the Arctic Ocean. *Global Biogeochemical Cycles*, *26*(4). https://doi.org/10.1029/2011GB004192

Terhaar, J., Lauerwald, R., Regnier, P., Gruber, N., & Bopp, L. (2021). Around one third of current Arctic Ocean primary production sustained by rivers and coastal erosion. *Nature Communications*, *12*(1), 1–10. https://doi.org/10.1038/s41467-020-20470-z

Torres, M. A., Limaye, A. B., Ganti, V., Lamb, M. P., Joshua West, A., & Fischer, W. W. (2017). Model predictions of long-lived storage of organic carbon in river deposits. *Earth Surface Dynamics*, *5*(4), 711–730. https://doi.org/10.5194/esurf-5-711-2017

Tsytovich, N. A. (1975). *Mechanics of frozen ground*. Scripta Book Co., McGraw-Hill.

University of Alaska Fairbanks Institute of Northern Engineering, District, U. S. A. C. of E. A., & Laboratory, U. S. A. C. of E. C. R. R. and E. (2019). Statewide threat assessment: Identification of threats from erosion, flooding, and thawing permafrost in remote Alaska communities. *Denali Commission*.

U.S. Army Corps of Engineers. (2007). *Alaska baseline erosion assessment: Erosion information paper—Huslia*. US Army Corps of Engineers.

Vandermause, R., Harvey, M., Zevenbergen, L., & Ettema, R. (2021). River-ice effects on bank erosion along the middle segment of the Susitna River, Alaska. *Cold Regions Science and Technology*, *185*, 103239. https://doi.org/10.1016/J.COLDREGIONS.2021.103239

Van De Wiel, M. J. (2003). *Numerical modelling of channel adjustment in alluvial meandering rivers with riparian vegetation*. University of Southampton.

Walker, H. J., Arnborg, L., & Peippo, J. (1987). Riverbank erosion in the Colville Delta, Alaska. *Geografiska Annaler—Series A: Physical Geography*, *69*(1), 61–70. https://doi.org/10.1080/04353676.1987.11880197

Wickert, A. D., Martin, J. M., Tal, M., Kim, W., Sheets, B., & Paola, C. (2013). River channel lateral mobility: Metrics, time scales, and controls. *Journal of Geophysical Research: arth Surface*, *118*(2), 396–412. https://doi.org/10.1029/2012jf002386

Wild, B., Andersson, A., Bröder, L., Vonk, J., Hugelius, G., McClelland, J. W., et al. (2019). Rivers across the Siberian Arctic unearth the patterns of carbon release from thawing permafrost. *Proceedings of the National Academy of Sciences of the United States of America*, *116*(21), 10280–10285. https://doi.org/10.1073/pnas.1811797116

Williams, J. R. (1952). Effect of wind-generated waves on migration of the Yukon River in the Yukon Flats, Alaska. *Science*, *115*(2293), 519–520. https://doi.org/10.1126/science.115.2993.519

Williams, J. R. (1955). Observations of freeze-up and break-up of the Yukon River at Beaver, Alaska. *Journal of Glaciology*, *2*(17), 488–495. https://doi.org/10.3189/002214355793702316

Williams, P. J., & Smith, M. W. (1991). The frozen earth.

Wohl, E., & Scamardo, J. E. (2022). Aufeis as a major forcing mechanism for channel avulsion and implications of warming climate. *Geophysical Research Letters*, *49*(20), e2022GL100246. https://doi.org/10.1029/2022GL100246

Woo, M. K., & Winter, T. C. (1993). The role of permafrost and seasonal frost in the hydrology of northern wetlands in North America. *Journal of Hydrology*, *141*(1–4), 5–31. https://doi.org/10.1016/0022-1694(93)90043-9

Woo, M. K. (1990). Consequences of climatic change for hydrology in permafrost zones. *Journal of Cold Regions Engineering*, *4*(1), 15–20. https://doi.org/10.1061/(asce)0887-381x(1990)4:1(15)

Woo, M. K., Kane, D. L., Carey, S. K., & Yang, D. (2008). Progress in permafrost hydrology in the new millennium. *Permafrost and Periglacial Processes*, *19*(2), 237–254. https://doi.org/10.1002/ppp.613

Yang, D., & Peterson, A. (2017). River water temperature in relation to local air temperature in the Mackenzie and Yukon basins. *Arctic*, *70*(1), 47–58. https://doi.org/10.14430/arctic4627

Young, B., Yarie, J., Verbyla, D., Huettmann, F., Herrick, K., & Chapin, F. S. (2017). Modeling and mapping forest diversity in the boreal forest of interior Alaska. *Landscape Ecology*, *32*(2), 397–413. https://doi.org/10.1007/s10980-016-0450-2

Zar, J. H. (1999). *Biostatistical analysis* (4th ed.). Prentice-Hall, Inc.

Zhang, T., Li, D., Kettner, A. J., Zhou, Y., & Lu, X. (2021). Constraining dynamic sediment-discharge relationships in cold environments: The sediment-availability-transport (SAT) model. *Water Resources Research*, *57*(10), e2021WR030690. https://doi.org/10.1029/2021WR030690

Zhao, K., Coco, G., Gong, Z., Darby, S. E., Lanzoni, S., Xu, F., et al. (2022). A review on bank retreat: Mechanisms, observations, and modelling. *Reviews of Geophysics*, *60*(2), 1–51. https://doi.org/10.1029/2021rg000761